Novel insights into old anticancer drugs

Zanden, S.Y. van der

Cover Page

Universiteit Leiden

Author: Zanden, S.Y. van der
Title: Novel insights into old anticancer drugs
Issue date: 2021-03-02
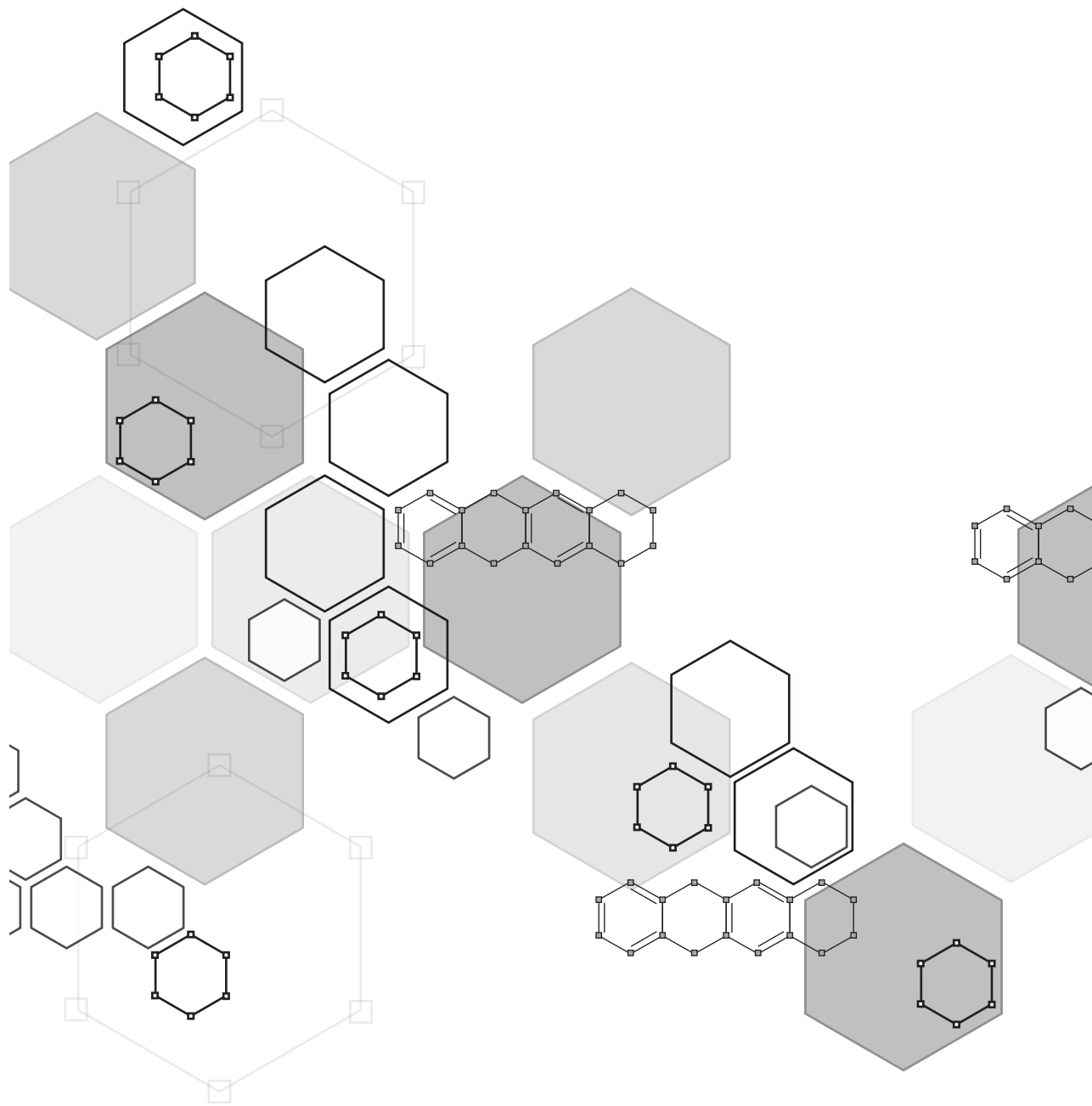
Uncoupling DNA damage from chromatin damage to detoxify doxorubicin

3

Sabina Y. van der Zanden[#], Xiaohang Qiao[#], Dennis P.A. Wander, Daniel M. Borràs, Ji-Ying Song, Xiaoyang Li, Suzanne van Duikeren, Noortje van Gils, Arjo Rutten, Tessa van Hewaarden, Olaf van Tellingen, Elisa Giacomelli, Milena Bellin, Valeria Orlova, Leon G.J. Tertoolen, Sophie Gerhardt, Jimmy J. Akkermans, Jeroen M. Bakker, Charlotte L. Zuur, Baoxu Pang, Anke M. Smits, Christine L. Mummery, Linda Smit, Ramon Arens, Junmin Li, Herman S. Overkleeft and Jacques Neefjes

#These authors contributed equally

ABSTRACT
The anthracycline doxorubicin (Doxo) and its analogs daunorubicin (Daun), epirubicin (Epi), and idarubicin (Ida) have been cornerstones of anticancer therapy for nearly five decades. However, their clinical application is limited by severe side effects, especially dose-dependent irreversible cardiotoxicity. Other detrimental side effects of anthracyclines include therapy-related malignancies and infertility. It is unclear whether these side effects are coupled to the chemotherapeutic efficacy. Doxo, Daun, Epi, and Ida execute two cellular activities: DNA damage, causing double-strand breaks (DSBs) following poisoning of topoisomerase II (Topo II), and chromatin damage, mediated through histone eviction at selected sites in the genome. Here we report that anthracycline-induced cardiotoxicity requires the combination of both cellular activities. Topo II poisons with either one of the activities fail to induce cardiotoxicity in mice and human cardiac microtissues, as observed for aclarubicin (Acla) and etoposide (Etop). Further, we show that Doxo can be detoxified by chemically separating these two activities. Anthracycline variants that induce chromatin damage without causing DSBs maintain similar anticancer potency in cell lines, mice, and human acute myeloid leukemia patients, implying that chromatin damage constitutes a major cytotoxic mechanism of anthracyclines. With these anthracyclines abstained from cardiotoxicity and therapy-related tumors, we thus uncoupled the side effects from anticancer efficacy. These results suggest that anthracycline variants acting primarily via chromatin damage may allow prolonged treatment of cancer patients and will improve the quality of life of cancer survivors.

SIGNIFICANCE
Anthracyclines like doxorubicin are anticancer drugs, used by over 1 million cancer patients annually. However, they cause severe side effects, most notably cardiotoxicity and therapy-related malignancies. It is unclear whether these side effects are directly linked to their anticancer activity. Doxorubicin exerts two activities: DNA damage and chromatin damage. Here, we show that both activities conspire the cardiotoxicity, while doxorubicin variants with only chromatin-damaging activity remain active anticancer drugs devoid of side effects. This challenges the concept that doxorubicin works primarily by inducing DNA double-strand breaks and reveals another major anticancer activity, chromatin damage. Translating these observations will yield anticancer drugs for patients that are currently excluded from doxorubicin treatment and improve the quality of life of cancer survivors.

INTRODUCTION
The anthracycline doxorubicin (also known as Adriamycin, Doxo) and its analogs daunorubicin (Daun), epirubicin (Epi), and Idarubicin (Ida) are widely used in the treatment of various hematologic malignances and solid tumors, as monotherapies or main ingredients in combination therapies with other drugs or antibodies [1, 2]. As many other chemotherapeutics, anthracyclines can cause severe side effects in patients, most notably dose-dependent irreversible cardiotoxicity, which can be lethal. Upon reaching the maximal cumulative dose, alternative treatment strategies are needed if any are available [3-5]. The risk of cardiotoxicity increases with age extremes [6] and also limits anthracycline treatment of recurring tumors, even if these drugs could still be effective [7-10]. As a result, elderly cancer patients with a 'weak heart' are often excluded from chemotherapy regimens containing anthracyclines

[11, 12]. Moreover, combination with other drugs or radiotherapy in the heart region further increases the incidence of anthracycline-related cardiotoxicity [13].

Besides cardiotoxicity, Doxo causes other serious side effects. Particularly devastating are therapy-related tumors [14, 15]. Roughly 1 to 3% of juvenile patients and 0.2 to 1% of breast cancer patients develop therapy-related tumors within 5 years after the initial anthracycline-containing treatment [16, 17]. Therapy-related tumors are frequently associated with high-risk cytogenetics with a significantly lower rate of complete remissions (CRs) than de novo tumors [18-20]. The third major side effect impacting quality of life is infertility [21]. Therefore, sperm or ova of young cancer patients are frequently collected and preserved prior to anthracycline-based chemotherapy for later fertility treatment.

It is unclear whether the anticancer activities of anthracyclines are intimately coupled to their various side effects. The anthracyclines are topoisomerase II (Topo II) poisons, whereby they induce DNA double-strand breaks (DSBs) [22]. While Doxo and related anthracyclines show high efficacy in the clinic, etoposide (Etop), a structurally unrelated Topo II poison which also generates DSBs [23], is significantly less potent in tumor control [24, 25] and less cardiotoxic [26]. This suggests that DNA damage as a result of Topo II poisoning does not fully account for the clinical effects and cardiotoxicity. More recently, anthracyclines unlike Etop have been shown to evict histones from particular regions in the genome [24, 27, 28]. Histone eviction by anthracyclines has multiple consequences, including epigenomic and transcriptional alterations and attenuated DSB repair, collectively referred to as chromatin damage [24, 29]. These studies identified a variant anthracycline, aclarubicin (Acla), that evicts histones but fails to induce DSBs [24, 29]. This drug is an effective anticancer drug, particularly for the treatment of acute myeloid leukemia (AML) [7, 30, 31].

Here, we reveal that the combination of DNA and chromatin damage assembled in Doxo and its variants is responsible for the different side effects. By understanding the effective chemical structure of each activity, we synthesized and identified analogs that failed to induce DSBs, but maintained histone eviction activity. These analogs abstained from causing therapy-related tumors and cardiotoxicity in mice and human cardiac microtissues, while retaining significant anticancer activity. It suggests that chromatin damage is apparently an important chemotherapeutic activity of anthracyclines, which—when separated from DSB formation—can ameliorate treatment-limiting side effects in mice. Consequently, anthracyclines can be detoxified by chemically removing the DNA-damaging effect while maintaining their chromatin-damaging activity. This provides different strategies for anthracycline development and a rationale for a more intense and broader application of anthracycline variants in the clinic.

RESULTS

The combination of DNA- and chromatin-damaging activities accelerates tumor formation and causes tissue toxicities in mice.

In addition to treatment-limiting cardiotoxicity, Doxo-containing chemotherapy induces treatment-related tumors in close to 1% of cancer survivors [16, 17]. To explore the molecular basis of the different side effects of anthracyclines, we tested the *in vivo* carcinogenicity and cardiotoxicity of Doxo, in parallel with its analog Acla, capable only of chromatin damage, and Etop—a nonanthracycline drug proficient in DSB induction via Topo II but incapable of chromatin damage [24]. Trp53$^{+/-}$ FVB mice [a spontaneous mouse tumor model [32-34]] were treated six times at two-week

intervals with Doxo, Acla, Etop, or saline at a drug dosage and treatment schedule corresponding to standard patient therapy [24, 35]. As in clinic practice, animals recovered from drug treatment within the two-week intervals, and no death was caused by acute toxicities. These mice were then followed for tumor development and long-term toxicities up to 72 weeks (Figure 1A). Doxo-treated mice presented accelerated death due to tumor formation, excluding 10 out of 32 Doxo-treated mice, who died from cardiotoxicity prior to development of detectable tumors. In contrast, Acla-treated mice showed attenuated spontaneous tumor formation, while Etop treatment moderately accelerated this process (Figure 1B and C). Since DNA mutations are a major driver of cancer [36], the difference in tumor formation for the three drugs could be a dose-dependent result of DNA errors introduced during inaccurate damage repair. Although Doxo and Etop both induce DSB, the damage is further exacerbated by the chromatin-damaging activity of Doxo [24]. Detailed histopathological analysis revealed that, among a variety of tumor types developed in Trp53$^{+/-}$ mice, high incidence of breast cancer was observed in 65% (11 out of 17) of Doxo-treated female mice, while the tumor spectra of Etop- and Acla-treated mice were comparable to that of saline-treated mice (SI Appendix, Table S1, Figure S1A and B). This observation may explain the increased risk for breast cancer observed in juvenile cancer survivors with a history of anthracycline-based therapies [37, 38]. Hence, the combination of DSB formation with chromatin damage induction, as for Doxo, enhances tumor formation, while removal of this, as for Acla, alleviates induction of therapy-related tumors.

Similar to human patients [3, 39], cumulative dose and male gender were also risk factors for Doxo-induced cardiotoxicity in mice (SI Appendix, Figure S1C–G). Histopathological analysis revealed substantial and exclusive heart damage in 78.1% of Doxo-treated mice, commonly presented as thrombus formation in the left atrium and auricle of the heart accompanied by inflammation and fibrosis [40, 41] (Figure 1D–F and SI Appendix, Figure S1H). Sirius Red staining highlights these lesion areas showing increased levels of collagen (Figure 1G and H), while further staining for desmin, vimentin and periostin showed impairment of myocytes (SI Appendix, Figure S2A and B) and increased fibrous stroma (SI Appendix, Figure S2C–I). Upregulation of periostin was also observed in the myocardium of ventricles in Doxo-treated mice, particularly in the left ventricles and septums (SI Appendix, Figure S2F and I). These alterations are known to be associated with anthracycline-induced chronic cardiotoxicity [42, 43]. Postmortem histopathological analysis of all other major organs revealed severe dose-dependent effects on spermatogenesis in Doxo-treated male mice only (Figure 1I and SI Appendix, Figure S2J–P), another known side effect of anthracyclines. These mouse experiments recapitulate three foremost long-term side effects of Doxo known in human patients and other animal models, suggesting that uncoupling DNA- from chromatin-damaging activity of anthracyclines could alleviate side effects, as this combination is absent in Etop and Acla.

Chromatin- and DNA-damaging activities can be uncoupled in anthracyclines. The anthracyclines Doxo, Daun, Epi and Ida all combine DNA-damaging and chromatin-damaging activities [24]. A recently developed anthracycline analog, amrubicin (Amr), was reported with limited cardiotoxicity [44]. We tested the DNA- and chromatin-damaging activities of Amr at physiologically relevant concentrations [24, 45]. DNA damage was visualized by constant-field gel electrophoresis (CFGE) [46, 47], comet assay [48] and phosphorylation of H2AX at Ser139 (γH2AX) [49]. Amr, Doxo, Daun, Epi, Ida and Etop all induced DSBs, unlike Acla (Figure 2A–E and

SI Appendix, Figure S3A–C). Subsequently, chromatin damage was detected after photo-activation of green fluorescent protein-labeled histone H2A (PAGFP-H2A) in living cells [24]. Only Amr and Etop failed to evict histones (Figure 2F and G and SI Appendix, Figure S3D and Movie S1). The anthracycline Amr thus mimicked Etop, which only induces DSBs. Amr and Etop both have limited cardiotoxicity [26, 44, 50],
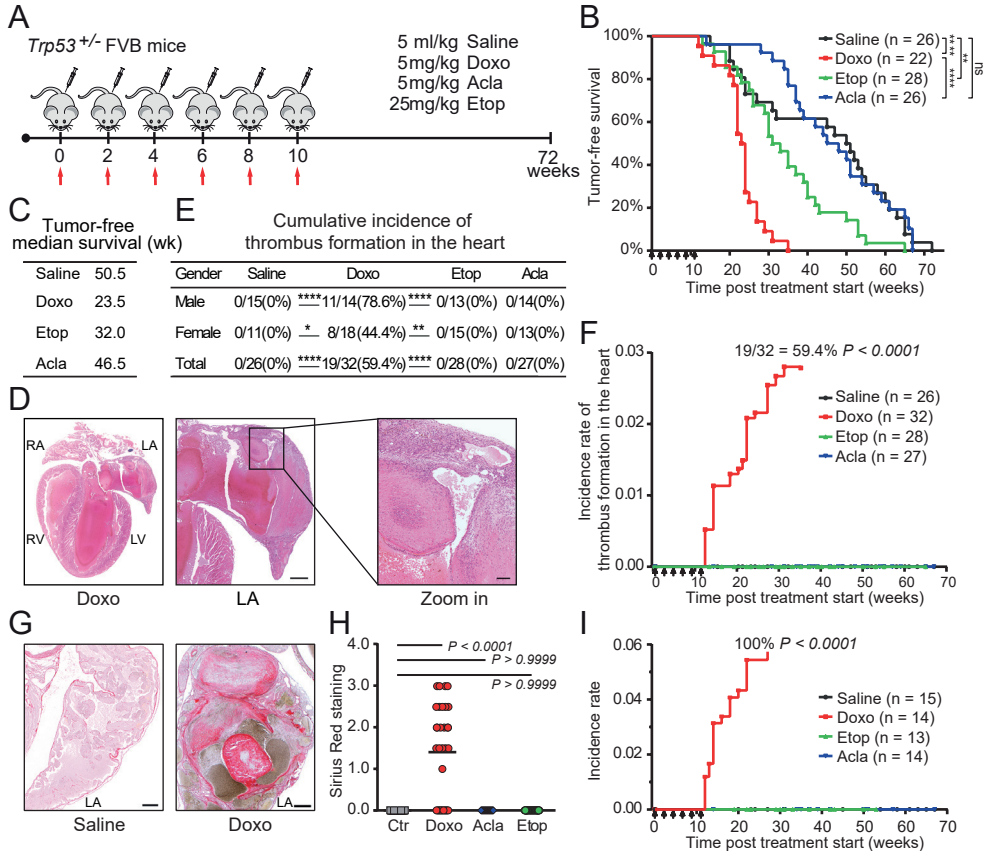
3

Figure 1. Doxo and Etop but not Acla accelerates tumor formation and causes tissue toxicities in Trp53$^{+/-}$ FVB mice. *(A) Trp53$^{+/-}$ FVB mice were i.v. injected with Doxo, Acla, Etop, or saline every two weeks for six times. Drug injections are indicated by arrows. (B) Tumor-free survival is plotted in a Kaplan-Meier curve. Log-rank test, ns, not significant; ****P < 0.0001; **P = 0.0093. (C) Tumor-free median survival of mice. (D) Representative microscopic images of the heart from Doxo-treated mouse with thrombosis formation in the left atrium/auricle. Higher magnifications shows thrombi and inflammatory lesions including fibrosis in the left auricle. LA = left atrium, RA = right atrium, LV = left ventricle, RV = right ventricle. Scale bars, 500 μm and 100 μm, respectively. (E) Cumulative incidence of thrombosis was analyzed for gender effect. Fisher's exact test, two-sided. *P < 0.05; **P < 0.01***; ****P < 0.0001. (F) The incidence rate of thrombus formation in the heart. Cumulative incidence is indicated next to the curve. Two-way ANOVA with RM, ****P < 0.0001. (G) Representative Sirius Red staining of the LA from saline- or Doxo-treated mouse. Scale bars, 100 μm. (H) Quantification of Sirius Red staining. Kruskal-Wallis test, ****P < 0.0001, Ctr vs Acla or Etop is ns. (I) Incidence rate of depletion of spermatogenesis in male mice. Cumulative incidence is indicated next to the curve. Two-way ANOVA with RM, ****P < 0.0001.*

again suggesting that DNA damage alone is insufficient to induce cardiotoxicity. Relocation of the amine group from the sugar (as found in Doxo) to the tetracycline moiety in Amr disabled histone eviction (Figure 2A), but still allowed induction of DSBs, suggesting that the amine on the sugar of Doxo is crucial for evicting histones. Furthermore, Acla whose amine group is present at the same position but in a dimethylated form exhibited only histone eviction activity without DSB induction (Figure 2A–G). To identify the structural basis of these two cellular activities of Doxo, we synthesized and tested *N,N*-dimethyldoxorubicin (diMe-Doxo) (Materials and Methods and SI Appendix, Method S1). *N,N*-dimethylation of the amine group in Doxo abolished DNA-damaging activity at various concentrations (Figure 2A–E and SI Appendix, Figure S3A–C), while still allowing histone eviction (Figure 2F and G and SI Appendix, Figure S3E–I and Movie S2). Further, the evicted H2B accumulated in the cytosolic fraction upon treatment of Doxo, diMe-Doxo and Acla but not for Amr and Etop (Figure 2H and I and SI Appendix, Figure S4A and B). The diMe-Doxo still relocated Topo IIα-GFP to chromatin (SI Appendix, Figure S4C), indicating that Topo IIα was trapped by the drug before the generation of DSB. These data suggest that manipulating the position and modification of the amine group in Doxo allows separation of the DNA-damaging and chromatin-damaging activities.

We then tested the relative contributions of DNA damage and chromatin damage to the anticancer effects of Doxo by assaying the cytotoxicity of these variants in different cancer cell lines (Figure 2J and K and SI Appendix, Figure S5A). The diMe-Doxo showed comparable or even superior effects in most cell lines tested compared to Doxo (14 out of 20), while Amr was poorly cytotoxic (Figure 2J). This increased potency of diMe-Doxo in these cell lines was unexpected, given that this compound lost its DNA-damaging activity. This enhanced potency could not be attributed to the rate of drug uptake as analyzed by flow cytometry following the autofluorescence of the anthracycline drugs (SI Appendix, Figure S5B). Reactive oxygen species (ROS) induced by anthracyclines was observed to be dose-dependent but only at late time point after drug removal (SI Appendix, Figure S6A and B), indicating that it could be a secondary effect of drug action. ROS can cause many vicious damages, which might be responsible for the cell death induced by anthracyclines. Although the different anthracyclines induced some increase in total ubiquitinated proteins, there was no significant difference observed for the different drugs (SI Appendix, Figure S6C and D). Besides ROS induction, chromatin damage induced cell death is probably executed by classical caspase-dependent apoptosis, as shown by PARP cleavage following exposure to these drugs (SI Appendix, Figure S6E and F).

Anthracyclines that only evict histones are effective in cancer treatment.
To assess the importance of chromatin damage for the clinical activity of anthracyclines, we performed a retrospective analysis in de novo geriatric AML patients, who were treated with either Ida-based (that induces both DSBs and chromatin damage) or Acla-based regimens (with chromatin damage only). Acla is reported to be equipotent to Daun for AML patients [30, 31], likewise Acla-based regimen resulted in comparable overall survival as Ida-based regimen (Figure 3A and SI Appendix, Figure S7A and Table S2 and S3), indicating that anthracycline drugs lacking DNA-damaging activity are effective in cancer treatment. The direct anticancer activity of diMe-Doxo compared to Doxo was evaluated *ex vivo* in primary human AML blasts (Figure 3B and C and SI Appendix, Figure S7B–H). Although some patient-to-patient variation existed, Doxo and diMe-Doxo were equally effective, while Acla appeared more cytotoxic in these dose-response experiments (Figure 3B and C and SI Ap-
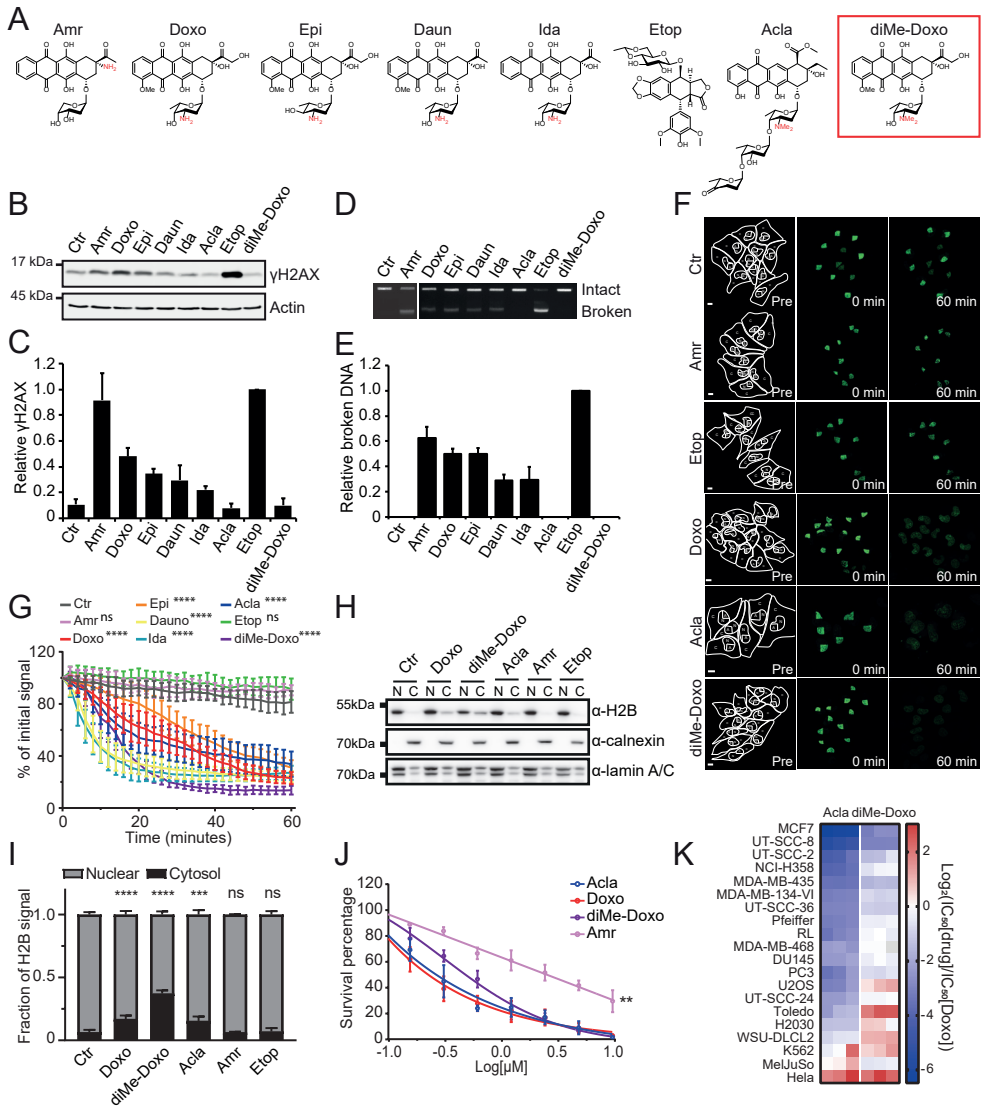
Figure 2. Evaluation of the DNA- and chromatin-damaging activities of anthracyclines.
*(A) Structures of Topo II poisons used in this study, the critical amine group in red. (B) K562 cells were treated for 2 hours with 10 µM of indicated drug. γH2AX levels were examined by Western blot. (C) Quantification of the γH2AX signal normalized to actin. (D) DSBs were analysed by CFGE. (E) Quantification of relative broken DNA in (D). (F) Part of the nucleus from MelJuSo-PAGFP-H2A cells was photo-activated. Photo-activated PAGFP-H2A was monitored by time-lapse confocal microscopy for 1 hour in the absence or presence of indicated drug at 10 µM. Lines in the left panel define the region of cytoplasm (C), nucleus (N) and activated area (A). Scale bar, 10 µm. (G) Quantification of the release of fluorescent PAGFP-H2A from the photo-activated region after drug administration. Two-way ANOVA, ****P < 0.0001. (H) Endogenously tagged scarlet-H2B U2Os cells were treated with 10 µM of the indicated drugs. Cells were fractionated and the nuclear versus cytosolic fraction of H2B was examined by Western blot. Calnexin was used as cytosolic, and lamin A/C as nuclear marker.*

Figure 2. Continued. *(I) The fraction of cytosolic versus nuclear H2B upon histone eviction by the drugs indicated is plotted. Two-way ANOVA, ***P < 0.001; ****P < 0.0001; ns, not significant. (J) Cell viability in K562 cells. Two-way ANOVA, Amr vs Doxo, diMe-Doxo or Acla, **P < 0.01. (K) Relative IC$_{50}$ values of each drug compared to Doxo in different cell lines.*
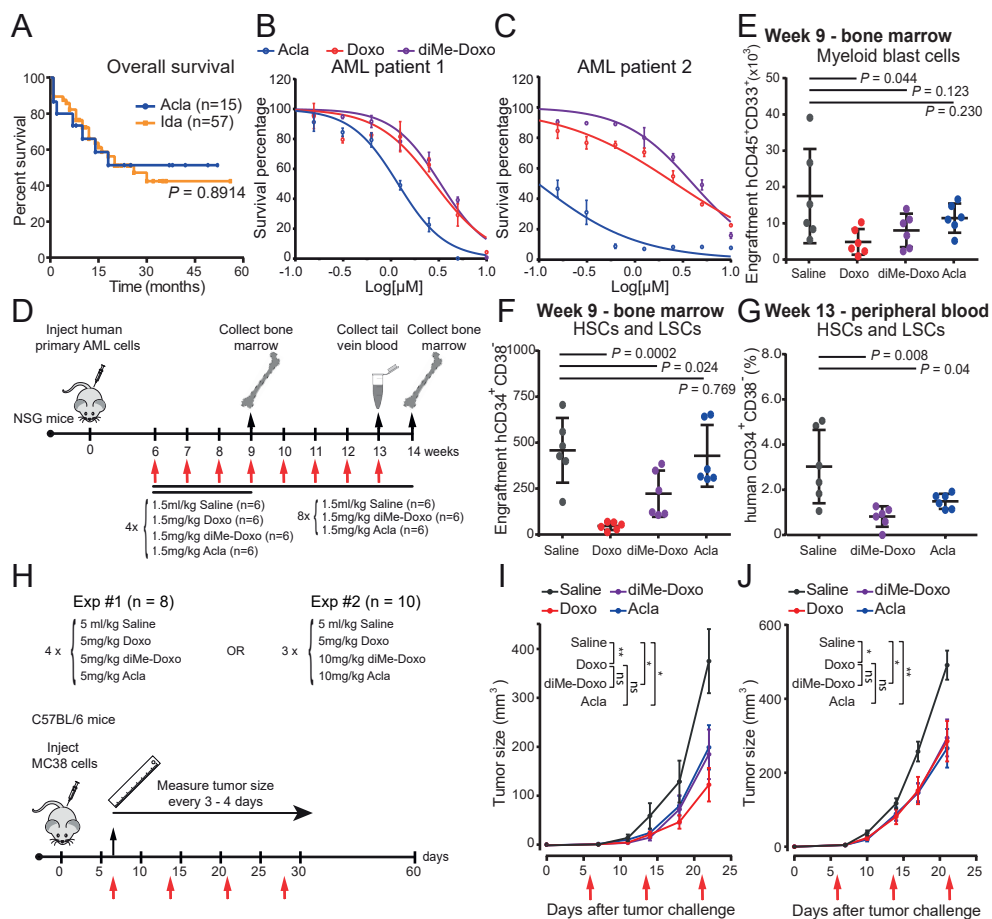

Figure 3. diMe-Doxo and Acla are effective anticancer drugs. *(A) Overall survival of de novo geriatric AML patients treated with a drug regimen including Acla or Ida. Log-rank (Mantel-Cox) test. (B) and (C) Dose-dependent cell viability of human AML samples, shown as mean ± SD of technical duplicates. (D) Schematic overview of AML PDX mouse experiment. (E) and (F) The engraftment of human AML cells in the bone marrow of the first cohort at week 9: absolute counts of myeloid blast cells (CD45$^+$CD33$^+$ blasts) (E) and HSCs and LSCs (CD34$^+$CD38$^-$ blasts) (F). Each symbol represents one mouse. Students' t-test. (G) The engraftment of human AML cells of the second cohort: the percentage of human HSCs and LSCs in peripheral blood at week 13. Students' t-test. (H) C57BL/6 mice were subcutaneously injected with MC38 cells. One week after tumor challenge, mice were treated with indicated drugs every week. Drug injections are indicated by arrows. (I) and (J) MC38 tumor growth following Exp #1 procedure (I) or Exp #2 procedure (J). One-way ANOVA, saline vs treatment, *P < 0.05; **P < 0.01.*

pendix, Figure S7B–H). Chromatin-damaging activity apparently contributes significantly to the cytotoxicity of Doxo in treating AML.

The anticancer activity of diMe-Doxo *in vivo* was tested in an AML patient-derived xenograft (PDX) mouse model [51] in comparison to Doxo and Acla (Figure 3D). Due to severe toxicity, mice treated with Doxo had to be killed after four courses of treatment at week nine, unlike mice treated with Acla or diMe-Doxo (SI Appendix, Figure S8A), which then received another four courses of treatment without any signs of toxicity (Figure 3D and SI Appendix, Figure S8B). At week nine, four courses of Doxo treatment significantly depleted human AML blast cells, hematopoietic stem cells (HSCs) and leukemic stem cells (LSCs) (Figure 3E and F and SI Appendix, Figure S8C), and it showed modest but not significant impact on normal mouse leukocytes (SI Appendix, Figure S8D). The diMe-Doxo and Acla did reduce the leukemic burden, albeit less efficient than Doxo (Figure 3E and F). With extended treatment of diMe-Doxo and Acla, most proliferating fractions of human hematopoietic cells were significantly reduced in mice (Figure 3G and SI Appendix, Figure S8E–H). The PDX experiment suggests that diMe-Doxo has the capacity to reduce the leukemic burden, the immature LSCs and leukemic progenitors *in vivo* with less hematopoietic toxicity compared to Doxo. Subsequently, we tested a solid colon carcinoma tumor mouse model for the efficacy of the different anthracyclines that either or not induce DSBs (Figure 3H). Both diMe-Doxo and Acla showed significant tumor control, although Doxo was slightly but not significantly better in reducing the tumor growth at equal dose (Figure 3I). A higher dose of diMe-Doxo and Acla resulted in equal tumor control (Figure 3J). Taken together, Acla or diMe-Doxo (with chromatin-damaging activity only) are effective anticancer drugs *in vitro* and *in vivo*, suggesting that chromatin damage could have a major contribution to the mechanism of anthracycline cytotoxicity.

N,N-dimethylation of Doxo prevents cardiotoxicity.

Since diMe-Doxo resembles the activity of Acla in terms of evicting histones while not causing DSBs (SI Appendix, Figure S9A), we wondered whether this also translates into reduced side effects. To address this, wild-type FVB mice were intravenously (i.v.) injected with Acla, Doxo or diMe-Doxo every two weeks (Figure 4A). Mouse body weight was monitored as a representative parameter of general toxicity prior to each injection [35]. While Doxo-treated mice significantly lost body weight and died from cardiotoxicity after eight injections, mice treated with diMe-Doxo remained healthy, with no weight loss or discomfort, even after 15 doses (Figure 4B and C and SI Appendix, Figure S9B). Histopathology demonstrated Doxo treatment induced severe cardiotoxicity as observed in Trp53^{+/-} FVB mice (Figure 1 and SI Appendix, Figure S1 and S2). None of the mice treated with either diMe-Doxo or Acla showed abnormalities in the heart (Figure 4C and SI Appendix, Figure S9C–J). The effects on cardiac function of mice was further evaluated by echocardiography. Doxo treatment resulted in a serious expansion of the left atrium with reduced fractional shortening (FS), left ventricular ejection fraction (EF), and cardiac output unlike any of the other treatments (Figure 4D–G and Movie S3). More direct (acute) cardiac cell damage and function impairment were assessed using human induced pluripotent stem cell (hiPSC)-derived cardiac microtissues [52-55]. Doxo unlike Acla or diMe-Doxo significantly affected contraction amplitude and contraction duration 24 hours posttreatment (Figure 4H and SI Appendix, Figure S9K–N and Movie S4). This suggested that cardiotoxicity can be the result from combining DNA and chromatin damage. This was directly tested by the combination of Amr (DNA damage only) and Acla (chromatin damage only) which reduced the contraction amplitude to some extend and significantly impaired the velocity of the microtissues, which reconstituted the
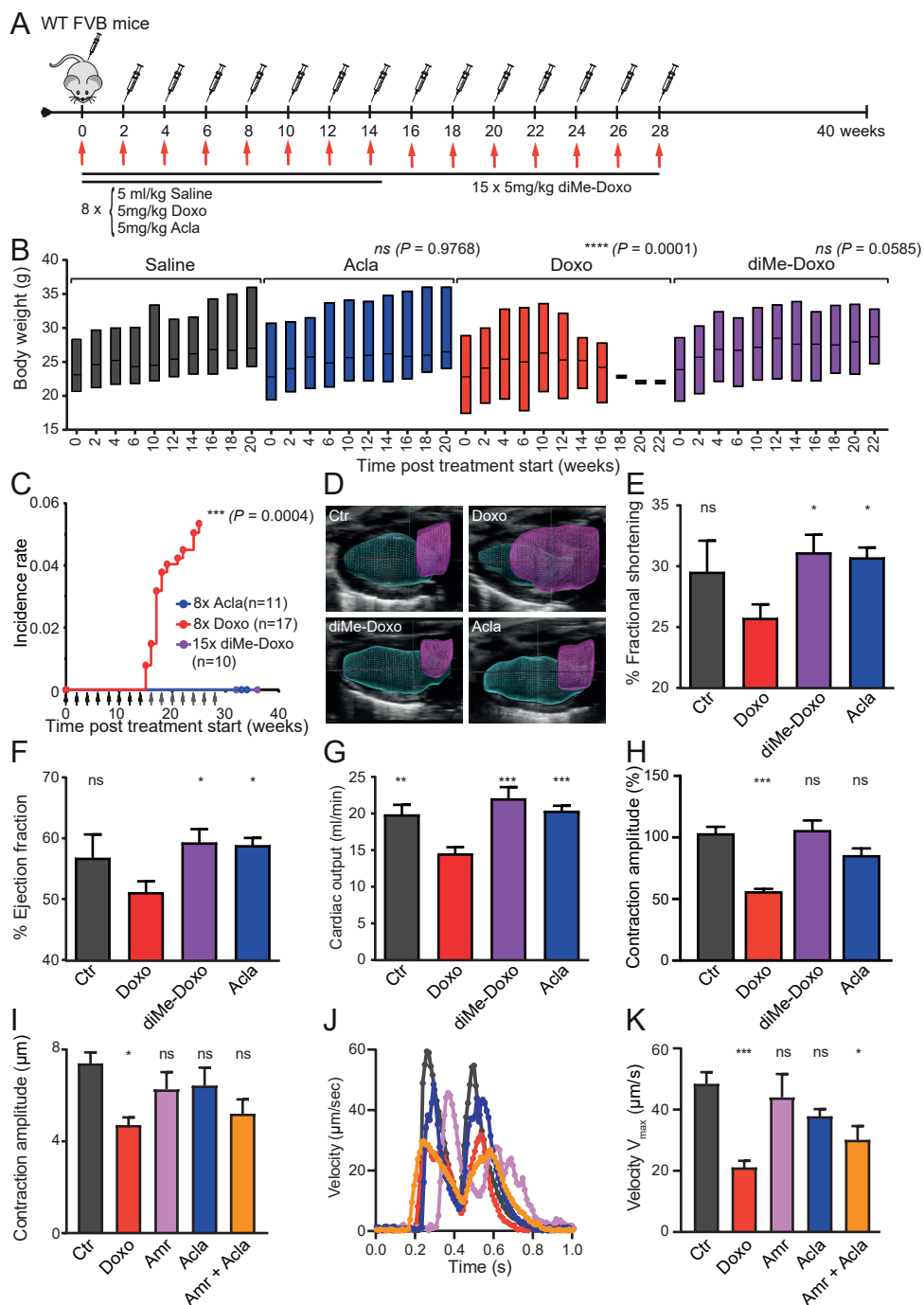
Figure 4. *N,N*-dimethylation of Doxo prevents cardiotoxicity in mice and hiPSC-derived cardiac microtissues. *(A–C), Wild-type FVB mice were i.v. injected with indicated drug every two weeks: Doxo or Acla for 8 times and diMe-Doxo for 15 times.*

Figure 4. Continued. *(B) The body weight of mice, shown as floating bars with maximum-median-minimum values. Two-way ANOVA with RM. (C) The incidence rate of cardiotoxicity. Arrows indicate drugs injections. Two-way ANOVA. (D–G) Cardiac function assessed by echocardiography 12 weeks post treatment start. FVB mice were treated for 8 times with saline (5 ml/kg, n = 5), Doxo (5 mg/kg, n = 8), diMe-Doxo (5 mg/kg, n = 6) or Acla (5 mg/kg, n = 9). (D) 3D reconstruction of the diastole heart by echocardiography. In the sagittal section the left ventricle (cyan) and left atrium (magenta) are highlighted. (E–G) Quantification of echocardiography, fractional shortening (E), left ventricular ejection fraction (F) and cardiac output (G). For (E-G) ordinary one-way ANOVA, Doxo vs saline, diMe-Doxo or Acla, *P < 0.05; **P < 0.01; ***P < 0.001; ns, not significant. (H) Drug toxicity on cardiac microtissues 24 hour post treatment. Contraction amplitude of microtissues treated with 20 μM of the different drugs. Krushal-Wallis test, *** P < 0.0002. (I-K) Drug toxicity on cardiac microtissues treated with single drugs or a combination of Amr and Acla, (I) Contraction amplitude of microtissues treated with the indicated single (20 μM) or combination drugs (10 μM + 10 μM). (J) Maximum velocity in μm/sec is indicated for a represented microtissue for the different treatments. (K) Quantification of the maximum velocity. For (I and K) ordinary one-way ANOVA, Ctr vs treatments; *P < 0.05; ***P < 0.001; ns, not significant.*

cardiotoxicity of Doxo in hiPSC-derived cardiac microtissues (Figure 4I–K). These differences in toxicity of the heart cannot be caused by a different biodistribution of the drugs, which was comparable for Doxo and diMe-Doxo (SI Appendix, Figure S9K and O). Unlike Acla, diMe-Doxo affected the male reproductive organs. The diMe-Doxo depleted spermatogenesis in all male mice and caused some Leydig cell hyperplasia but to a lesser extent than its parental drug Doxo, even at higher cumulative dose (SI Appendix, Figure S9P and Q). Significant toxicity in ovaries in young mice at early time points was observed only for Doxo-treated mice, shown as increased apoptosis in secondary and tertiary follicles (SI Appendix, Figure S9R–T). These results indicated that diMe-Doxo or Acla (with chromatin-damaging activity only) are less toxic than anthracyclines that induce both DNA and chromatin damage (such as Doxo), while remaining effective anticancer drugs.

DISCUSSION

About one million cancer patients annually receive treatment with Doxo or its analogs Daun, Epi, or Ida. Unfortunately, anthracyclines cause severe side effects, particularly cardiotoxicity [3, 4]. This side effect excludes (often elderly) patients with compromised heart function from receiving effective cancer treatments [56]. Understanding and ultimately eliminating the root causes of this and other side effects of anthracyclines would thus greatly expand the application of these drugs in cancer treatment.

It has been suggested that ROS formation may be responsible for cardiotoxicity induced by anthracyclines [57, 58]. However, co-administration of radical quenchers during anthracycline treatment did not ameliorate cardiotoxicity in clinical studies [59, 60]. Moreover, high redox potential of Acla relative to that of Doxo or Daun [61] does not match Acla's lack of cardiotoxic effects. Our data also show that Acla and diMe-Doxo produce more ROS compared to Doxo (SI Appendix, Figure S6A), rather suggesting that ROS induction cannot explain the differences in cardiotoxicity of anthracyclines studied here. Mechanistically, cardiotoxic anthracyclines, such as Doxo, Daun, Epi, and Ida, constitute multifunctional agents capable of DNA damage (by poisoning Topo II and DSB formation) combined with chromatin damage (via histone eviction). The anticancer effects have been attributed to DNA damage, but the variants unable to induce DNA damage show equal anticancer potency in AML treatment. While therapy-related tumors can be understood as the consequence

of delayed and unfaithful DNA damage repair [24], the cause of cardiotoxicity by anthracyclines is still unsolved. Failure of removing cardiotoxicity by chemical modification in the past led to different delivery strategies such as liposome-encapsulated Doxo, but with modest improvement and limited use in clinical practice [62]. Here we show that cardiotoxicity associated with Doxo is alleviated in mice treated with drugs that either induce DSBs (Etop) or evict histones (Acla, diMe-Doxo). This effect is further confirmed in hiPSC-derived cardiac microtissues and by echocardiography, collectively implying that the combination of DNA and chromatin damage induces cardiotoxicity. Although Doxo is an exceptional drug that shows very similar pharmacokinetics in human and mouse [63], there remain some distance between our mouse models and humans. However, the long-term toxicities of Doxo, cardiotoxicity, infertility and therapy-related tumorigenesis, observed in our mouse models do correlate very well with clinical observations. With this promising result from mice, effort will be made to test this concept in other animal models and clinical trial.

Many chemical variations of anthracyclines have been synthesized before, including diMe-Doxo [64, 65]. However, these drugs were only tested for their ability to induce DNA damage, which was considered the main mechanism of therapeutic efficacy for anthracyclines [66]. Since chromatin damage was unknown at that time [24], many of the variants lacking DNA-damaging activity were not further developed. We propose that, by further understanding the cellular activities of anthracyclines, detoxification of Doxo is possible, which only requires a minimal chemical modification to remove the DNA-damaging activity. Such drugs would allow more intense treatment of primary tumors and continuous anthracycline treatment of relapsed tumors. Additionally, patients with higher cardiotoxicity risk, who are now excluded from anthracycline-based cancer treatments, may benefit from the detoxified anthracyclines. Evaluating old anticancer drugs with modern technologies may lead to better understanding of drug activities (such as chromatin damage) that could then provide new strategies for improvement of cancer therapies as exemplified—in this case—by diMe-Doxo. Chemical dissection of the cellular activities of Doxo uncovered a new mechanism of action for anthracyclines—chromatin damage—an effective anticancer drugs devoid of the most critical side effects of anthracyclines.

MATERIALS AND METHODS
Reagents
Doxo and Etop were obtained from Pharmachemie (the Netherlands). Daun was obtained from Sanofi-Aventis (the Netherlands). Epi was obtained from Accord Healthcare Limited (UK). Acla for *in vivo* mouse experiment was purchased from Shenzhen Main Luck Pharmaceuticals Inc. (China). All the drugs were dissolved according to the manufacturer's formulation. Amr (sc-207289), Acla (sc-200160, for *in vitro* experiments), and Ida (sc-204774) were purchased from Santa Cruz Biotechnology (USA), dissolved in dimethylsulfoxide at 5 mg/ml concentration, aliquoted and stored at −20°C for further use.

Synthesis of *N,N*-dimethyldoxorubicin
All chemicals were used as received unless stated otherwise. ^{1}H and ^{13}C NMR spectra were recorded on a 400/100 or 500/125 NMR spectrometer. Chemical shifts (δ) are given in parts per million relative to tetramethylsilane (TMS) as internal standard. Coupling constants are given in hertz. All given ^{13}C spectra are proton decoupled. Spin multiplicities are given as s (singlet), d (doublet), dd (doublet of doublets), ddd (doublet of doublet of doublets), dt (doublets of triplets), t (triplet), td (triplet

of doublets), q (quartet), dq (doublet of quartets), qd (quartet of doublets), h (heptet), and m (multiplet). All individual signals were assigned using two-dimensional (2D) NMR spectroscopy, HH-COSY (proton-proton correlated spectroscopy), and heteronuclear single quantum correlation. Flash chromatography was performed on Screening Device B.V. silica gel 60 (0.04−0.063mm). TLC analysis (on Merck silica gel F254 plates) was followed by detection by ultraviolet absorption (254nm) where applicable and by spraying with a solution of $(NH_4)_6Mo_7O_{24} \cdot H_2O$ (25 g/L) and $(NH_4)_4Ce(SO_4)_4 \cdot 2H_2O$ (10 g/L) in 10% sulfuric acid in water followed by charring at 275°C. Liquid chromatography-mass spectrometry (LC-MS) standard eluents used were A: 100% H_2O, B: 100% acetonitrile, and C:1% TFA in H_2O. A C18 column (4.6 mm D×50 mm L, 3 μ particle size) was used. All analyses were 13 minutes, at a flow-rate of 1 mL/min. High-resolution mass spectra were recorded on a LTQ-Orbitrap equipped with an electrospray ion source in positive mode (source voltage 3.5 kV, sheath gas flow 10, capillary temperature 275°C) with resolution R = 60.000 atm/z= 400 (mass range = 150−4000) and dioctylphtalate (m/z = 391.28428) as "lock mass". Size exclusion chromatography was performed on Sephadex LH20 (eluent MeOH/DCM, 1:1). Detailed synthesis schemes can be found in the SI Appendix, Methods S1.

Cell culture
K562 (B. Pang, Stanford University, Stanford, CA), THP-1 (ATCC, Manassas, VA), DU145 (C. Robson, Newcastle University, Newcastle, United Kingdom), NCI-H358, MBA-MD-468 (R. Bernards, Netherlands Cancer Institute [NKI], Amsterdam, The Netherlands), and Pfeiffer cells (ATCC, Manassas, VA) were maintained in RPMI-1640 medium supplemented with 8% FCS. MCF-7 (W. Zwart, NKI, Amsterdam, The Netherlands), U2OS cells (M. Innocenti, NKI, Amsterdam, The Netherlands) and MC38 cells (M. Colonna, Washington University School of Medicine, St. Louis, MO) were cultured in Dulbecco's Modified Eagle's medium (DMEM) supplemented with 8% FCS. MelJuSo cells were cultured in Iscove's Modified Dulbecco's medium (IMDM) supplemented with 8% FCS. UT-SCC-8 cells (R. Grenman, University of Turku, Turku, Finland) were cultured in DMEM medium supplemented with 8% FCS and 1% non-essential amino acid. MelJuSo cells stably expressing PAGFP-H2A, PAGFP-H3 or PAGFP-H4 were maintained in IMDM supplemented with 8% FCS and G-418, as described [24]. MelJuSo cells were transiently transfected with a construct encoding Topo IIα-GFP [24]. Endogenous tagged scarlet-H2B cells were generated using homology repair scarlet constructs, which was designed 250 base pairs upstream and downstream of the genomic H2BC11 region. The guide RNA (gRNA) target sequence was designed by the CRISPOR tool and cloned into the pX330 Cas9 vector. Primers used for the homologous recombination (HR) construct: H2B homology arm left fwd: CCCACATATGCAAGGTTCTGAAGCAGGTCCAC; H2B homology arm left rev: CCCAGCTAGCCTTAGCGCTGGTGTACTTGG; H2B homology arm right fwd: CCCAGGTACCACAGTGAGTTGGTTGCAAAC; H2B homology arm right rev: CCCAGGATCCAACTTATAATAGAAAATTTCCCATCTCC. Primers used for the pX330 Cas9 vector: H2B gRNA fwd: CACCGACTCACTGTTTACT-TAGCGC; H2B gRNA rev: AAACGCGCTAAGTAAACAGTGAGTC. All cell lines were maintained in a humidified atmosphere of 5% CO_2 at 37°C and regularly tested for the absence of mycoplasma.

Primary human AML cells isolation and culture
All studies were conducted in accordance with the Declaration of Helsinki, and the

full study protocol was approved by the Ethics Committee of the Vrije Universiteit Medical Center (VUmc). At diagnosis, bone marrow (BM) or peripheral blood (PB) from AML patients hospitalized at the VUmc in Amsterdam, The Netherlands was collected with informed consent and according to protocols approved by the Ethics Committee of the VUmc. Mononuclear cells were isolated using Ficoll-Paque Plus (Amersham Biosciences, Uppsala, Sweden). Primary AML cells were kept in IMDM supplemented with 15% BIT9500 (Stemcell Technologies), Pen-Strep, 50 ng/ml human FLT3 ligand, 20 ng/ml human IL3 and 100 ng/ml human stem cell factor (PeproTech).

Mouse experiments for assessing drug toxicities

Mice were housed in individually ventilated cages (IVC) under specific pathogen-free (SPF) conditions in the animal facility of the NKI (Amsterdam, The Netherlands). All mouse experiments were performed according to institutional and national guidelines and were approved by the Animal Ethics Committee of the NKI (Amsterdam, The Netherlands). $Trp53^{+/-}$ or wild-type FVB mice were bred by the NKI mouse facility. $Trp53^{+/-}$ FVB mouse strain and genotyping protocol were as described [32]. Mice (10 wk to 11 wk old) were i.v. injected with 5 mg/kg of Doxo, 5 mg/kg of Acla, 5 mg/kg of diMe-doxo, 25 mg/kg of Etop or 5 mL/kg of saline every two weeks for the indicated times. Then tumor formation and animal welfare (weight loss, lethargy, hunched posture, poor grooming [rough hair coat]) were monitored every other day. When the tumor diameter exceeded 1 cm or the body-weight loss was more than 20%, the animal was euthanized by CO_2. Subsequently all organs and tumors were collected, fixed in EAF fixative (ethanol/acetic acid/formaldehyde/saline at 40:5:10:45 v/v), and embedded in paraffin. Sections were cut at 2 µm from the paraffin blocks and stained with hematoxylin and eosin, Sirius Red or indicated antibodies according to standard procedures. Primary antibodies were: Desmin (1:200, M 0760, DakoCytomation), Vimentin (1:100, #5741, Cell Signaling) and Periostin (1:100, ab215199, Abcam). The pathology slides were reviewed by an expert mouse pathologist who was blind to the treatment. Incidence rate (IR = [number of mice with specific side effect over a time period] / [sum of mice x time at risk during the same time period]) and cumulative incidence (CI = [number of mice with specific side effect at end time point] / [total number of mice at start]) were calculated for indicated side effects.

Pharmacokinetics of anthracyclines in FVB mice

Mice were housed in individually ventilated cages (IVC) under specific pathogen-free (SPF) conditions in the animal facility of the NKI (Amsterdam, The Netherlands). All mouse experiments were performed according to institutional and national guidelines and were approved by the Animal Ethics Committee of the NKI (Amsterdam, The Netherlands). Wild-type FVB mice were bred by the NKI mouse facility. Female mice (8 wk old) were i.v. injected with 5 mg/kg of Doxo, 5 mg/kg of Acla or 5 mg/kg of diMe-doxo, with five mice per group. Four hours post injection, animals were killed, and then heart, liver, kidney, spleen, reproductive organ, and plasma was collected. Hearts were cut into two pieces with coronal section. One piece was fixed in EAF for γH2AX staining. The other half of the heart and the rest of organs were weighed and frozen for the pharmacokinetics study. Doxo was measured by high performance liquid chromatography fluorescence detection as described before [67]. Acla and diMe-Doxo were analysed by LC-MS/MS. Sample pretreatment involved protein precipitation with acetonitrile: formic acid (99:1) containing 500 nM of Doxo as internal standard, followed by centrifugation (5 min, 20,000 g) and dilution of the supernatant

with water (1:3). Samples were centrifuged again and an aliquot of 50 µl was injected into the LC-MS/MS system. Separation was done using an Extend C18 column (100 x 2.1 mm). Mobile phase A (0.1% formic acid in water) and B (methanol) was delivered at 0.4 ml/min at 20% B. Following injection, a linear gradient to 95% B in 2.5 min was applied, kept at 95% for 2 min and then returned to 20% B. The API4000 MS (Sciex) was used in MRM mode; Acla: 812.5/333.1; diMe-Doxo: 571.9/99.9; and Doxo: 544.4/86.1).

PDX mouse model for AML

Mice were housed in IVC under SPF conditions in the animal facility of the VUmc (Amsterdam, The Netherlands). PDX mouse experiments were performed according to institutional and national guidelines and were approved by the Animal Ethics Committee of the VUmc (Amsterdam, The Netherlands). NOD/SCID/IL2r gamma null (NSG) mice (Jackson Laboratory) (6 wk to 8 wk old) were i.v. injected with 0.7×10^6 primary human AML cells per mouse 24 hours post 200-cGy total irradiation. PB was taken via the tail vein and analyzed by flow cytometry for human AML cells, defined by > 0.7% of hCD45+ cells. Six weeks after AML injection, mice were i.v. injected with 1.5 mg/kg of drug or saline weekly for the indicated times. Animals were monitored every other day. PB was taken from the tail vein and analyzed by flow cytometry at week 13. After killing, the hearts were collected for histopathological analysis, and BM was analyzed by flow cytometry.

MC38 colon carcinoma mouse model

Mice were housed in IVC under SPF conditions in the animal facility of Leiden University Medical Center (LUMC, Leiden, The Netherlands). Experiments were performed according to institutional and national guidelines and approved by the Animal Ethics Committee of the LUMC (Leiden, The Netherlands). C57BL/6 female mice obtained from Charles River Laboratories, 8 wk to 10 wk old, were subcutaneously (s.c.) injected with 3×10^5 MC38 cells in the right flank of the mice. Tumor size was measured every 3 to 4 days using a caliper. Mice were i.v. or retro-orbitally injected with indicated doses of Doxo, Acla, diMe-doxo or 5 mL/kg of saline every week for the indicated times. Mice were monitored twice per week. When the tumor exceeded 500 mm^3 or the body-weight loss was more than 20%, the animal was killed by CO_2. Then the heart, reproductive organ, and tumor were collected, fixed in EAF fixative (ethanol/acetic acid/formaldehyde/saline at 40:5:10:45 v/v) and embedded in paraffin for histopathological analysis.

Echocardiography

Mice were housed in IVC under SPF conditions in the animal facility of the LUMC (Leiden, The Netherlands). Experiment was performed according to institutional and national guidelines and approved by the Animal Ethics Committee of the LUMC (Leiden, The Netherlands). Both male and female FVB N/ctr mice (8 wk old), were i.v. injected with 5 mg/kg of Doxo, 5 mg/kg of Acla, 5 mg/kg of diMe-doxo or 5 mL/kg of saline every week for eight times. Animal welfare was monitored every other day. *In vivo* cardiac function was assessed by transthoracic echocardiograph. Mice were anesthetized with 2% isoflurane, depilated, and imaged in a supine position using a Vevo 3100 high-resolution ultrasound system, equipped with a 40-MHz center frequency linear array transducer (MX550D, FUJIFILM VisualSonics Inc., Toronto, Canada). Body temperature was kept at 37ºC, cardiac frequency was monitored with ECG and maintained between 400-600bpm. B-mode and M-mode echocardio-

graphic images were obtained in short-axis (SAX) view at the mid-papillary muscle level. Data were analyzed offline using VevoLAB software (FUIJIFILM VisualSonics, Toronto, Canada) and left-ventricular function was assessed using ejection fraction (EF) and fractional shortening (FS) of at least 3 cardiac cycles on SAX M-mode. To reconstruct the dimensions of the left ventricle and left atrium, 4D ultrasound imaging was performed by clamping the probe on a linearly translating step motor and positioning it parallel to the short axis of the left ventricle. System-integrated triggering between the motor and the probe resulted in automatically acquired high frame rate (300 fps) cardiac- and respiratory-gated cine loops with a 200 µm step size covering apex to base, that were spatiotemporally compiled into 4D data. 3D images of the left ventricle and atrium were constructed by manual tracing offline using VevoLAB software (FUIJIFILM VisualSonics, Toronto, Canada).

Western blot and CFGE
Cells were treated with drugs at indicated doses for 2 hours. Subsequently, drugs were removed by extensive washing, and cells were collected at indicated time points after drug removal and processed immediately for the assay. Cells were lysed directly in SDS-sample buffer (2% SDS, 10% glycerol, 5% β-mercaptoethanol, 60 mM Tris-HCl pH 6.8 and 0.01% bromophenol blue). Lysates were resolved by SDS/polyacrylamide gel electrophoresis followed by Western blotting. Primary antibodies used for blotting: γH2AX (1:1000, 05-036, Millipore), β-actin (1:10000, A5441, Sigma), ubiquitin (1:500, P4D1, sc-8017, Santa Cruz), alpha-tubulin (1:5000, 11223-1-AP, Protein tech). DNA double-strand breaks were quantified by constant-field gel electrophoresis, as described [46]. Images were quantified with ImageJ.

Fractionation assay
Endogenously tagged scarlet-H2B cells were treated for 1 hour with 10 µM of the indicated drugs. Cells were washed and lysed directly in lysis buffer (50mM Tris-Hcl pH 8.0, 150 mM NaCl, 5 mM $MgCl_2$, 0.5% NP40, 2.5% glycerol supplemented with protease inhibitors, 10 mM NMM and 10 µM MG132), collected, vortexed and incubated for 10 min on ice. To collect the cytosolic fraction samples were centrifuged for 10 minutes, 15000g, 4°C. Both nuclear (pellet) and cytosolic (supernatant) fractions were washed and prepared for Western blot analysis. Primary antibodies used for blotting: RFP (1:2000, 6G6, Chromotek), Lamin A/C (1:500, sc-20681, Santa Cruz), Calnexin (1:1000, C5C9, Cell signaling).

Comet assay
Neutral comet assays were performed as described by Olive and Banath [48]. Pictures of individual cells were taken with a Zeiss AxioObserver Z1 inverted microscope equipped with a cooled Hamamatsu ORCA AG Black and White CCD camera and analyzed with CASP software 1.2.3b2 (http://casplab.com/).

Microscopy
Cells stably expressing PAGFP-H2A, PAGFP-H3, or PAGFP-H4 were used for histone eviction experiments. Photoactivation and time-lapse confocal imaging were performed as described [24]. All live cell imaging experiments were analyzed by a Leica SP8 confocal microscope system, 63x lens, equipped with a climate chamber. Loss of fluorescence from the photoactivated region after different treatments was quantified using ImageJ software. For cytosolic H2B detection, endogenous tagged scarlet-H2B cells were seeded on coverslips. Upon treatment with 10 µM

of the indicated drugs for 1 hour, cells were fixed in paraformaldehyde (PFA) 4%, permeabilized with 0.1% Triton, and stained with anti-RFP (1:100, 6G6, Chomotek), goat-anti-mouse-Alexa Fluor 488 (1:400, Thermo fisher Scientific) and Alexa Fluor 647 phalloidin (1:125, A22287, Thermo fisher Scientific). Cells were analyzed by a Leica SP8 confocal microscope system, 63x lens. Cells were quantified using ImageJ software.

Cell viability assay
Indicated tumor cells or AML patient cells were seeded into 96-well plates. Twenty-four hours after seeding, cells were treated with indicated drugs for 2 hours at concentrations corresponding to physiological levels of cancer patients at standard treatment [24]. Subsequently, drugs were removed and cells were left to grow for an additional 72 hours. Cell viability was measured using the CellTiter-Blue viability assay (Promega). Relative survival was normalized to the untreated control and corrected for background signals.

Flow cytometry for measuring drug uptake in cells
Cells were treated with 1 µM of drug for the indicated time points. Samples were washed, collected, and fixed with paraformaldehyde. Samples were analyzed by flow cytometry using BD FACS aria II, with 561 nm laser and 610/20 nm detector. Drug uptake was quantified using FlowJo software.

Detection of ROS
MelJuSo cells were treated with indicated drugs for 2 hours followed by drug removal. Cells were collected immediately or 1 day after drug removal for analysis. Cells were then incubated with 10 µM of 2',7'-dichlorodihydrofluorescein diacetate (H2DCFDA) (Invitrogen, D399) for 30 min at 37 °C in the dark, and fluorescence was analyzed with an LSRFortessa™ flow cytometer (BD Biosciences). Mean fluorescence intensity of H2DCFDA was quantified using FlowJo software.

Flow cytometry for phenotyping AML cells
Human AML cells were treated with indicated drug for 2 hours, followed by extensive washing. Three days later, the cells were stained with anti-CD45-V500 (2D1, BD Bioscience, 1:20), anti-CD34-BV421 (581, BD Bioscience, 1:20), anti-CD38-APC (HB7, BD Bioscience, 1:50), anti-CD33-PE-Cy7 (p67.6, BD Bioscience, 1:20), anti-CD3-PE (SK7, BD Bioscience, 1:50), anti-CD19-APC-H7 (SJ25C1, BD Bioscience, 1:10), 7AAD (BD Bioscience, 1:10) and anti-CD11b-FITC (Bear1, BD Bioscience, 1:10) or anti-CD7-FITC (M-T701, BD Bioscience, 1:20) for 30 minutes. 15 µl of well-suspended flow count fluorospheres (Beckman Coulter) were added right before analyzed by flow cytometry with BD Fortessa™.

Assessing drug toxicity on hiPSC-derived cardiac microtissues
hiPSC-derived cardiac microtissues composed of hiPSC-derived cardiomyocytes and hiPSC-derived cardiac endothelial cells were generated as described [52, 53], with addition of stromal cells derived from hiPSC-epicardial cells, differentiated in monolayer as described [54]. For contraction analysis, microtissues were seeded on a Matrigel-coated 96-well plate (plastic, Black/Clear tissue culture treated plate) and imaged 24 hour post drug treatment with 20 or 30 µM of the indicated drugs. The Horn-Schunck Vector Flow analysis method was used to detect changes in pixel displacements during contraction of the microtissues. The analysis package was

developed with LabVIEW Motion and Vision (National Instruments). Images were collected at 100 frames per second with a Thor Labs camera DCC3260M (Thorlabs GmbH 85221) and a 10x objective phase contrast objective (Leica Inverted micro-scope IBDE). Microtissues were perfused with Tyrode's solution at 37 ºC and paced at 1 Hz. Tyrode's solution contains: 140 mM NaCl, 5.4 mM KCl, 1.8 mM $CaCl_2$, 1.0 mM $MgCl_2$, 5.5 mM glucose and 5.0 mM HEPES; pH 7.4 (NaOH).

AML patient data analysis
Patients with de novo geriatric AML treated between January 2014 and January 2019 in Ruijin Hospitals were enrolled in this retrospectively study. This study was approved by the ethics committee of Ruijin Hospital, and all patients provided writ-ten informed consent. Patients in the Acla group were treated with CAG regimen (Ara-C 15–25 mg/m^2 injected subcutaneously every 12 hours on day 1–14, Acla 20 mg/day infused intravenously on day 1–4, and granulocyte stimulating factor (G-CSF) 200 $\mu g/m^2$ administered s.c. daily on day 1 to 14). G-CSF was reduced, or temporarily stopped when neutrophilia was >5×10^9/L. Patients of Ida group were treated with IA regimen (Ida 6–10 mg/m^2/day infused i.v. on day 1 to 3 and Ara-C 100-200 mg/m^2 per day on day 1 to 7). Cytogenetic risk was classified according to the modified Southwest Oncology Group criteria [68]: 1) favorable risk, includ-ing t(8;21) and inv(16) or t(16;16)(p13;q22); 2) unfavorable risk, including del(5q) or monosomy 5, monosomy 7 or del(7q), abnormal 3q, 9q, 11q, 21q, or 17p, t(6;9), t(9;22), and complex karyotypes (three or more unrelated chromosomes abnormal); and 3) intermediate risk, including normal karyotypes and all other anomalies. Muta-tions in the NPM1 and CEBPA, and for FLT3 internal tandem duplication (FLT3-ITD), were tested. Integrated risk was classified according to ref. [69]. Complete remission (CR) was defined <5% blast cells in normocellular BM, PB counts showing neutro-phils ≥1×10^9/L and platelet count ≥100×10^9/L, and the disappearance of all clinical signs of leukemia. Partial remission (PR) was defined as having <15% (and a 50% decrease in BM blasts) but >5% blasts or with <5% blasts but not reaching the CR criteria for blood cell count or clinical manifestation. For analysis of CR, missing data were imputed as no CR. The baseline characteristics and clinical outcomes of the patients are summarized in SI Appendix Table S2 and S3, respectively.

Quantification and statistical analysis
Each sample was assayed in biological triplicate, unless stated otherwise. All error bars denote SD. Statistical analyses were performed using Prism 7 and 8 software (Graphpad Inc.). Student's t-test was used to compare two groups of independent samples. One-way ANOVA was used to compare more than two groups of independ-ent samples. Two-way ANOVA with repeated measure analysis was used if the re-sponse of two drugs was compared over time. Kaplan-Meier analysis and Log-rank (Mantel-Cox) test were used to evaluate the statistical significance for comparison of survival curves. Western blot and confocal data were quantified using ImageJ software. Significance is represented on the graphs as follow: ns, not significant; *$p < 0.05$; **$p < 0.01$; ***$p < 0.001$; ****$p < 0.0001$. No statistical methods were used to predetermine sample size.

Data availability
All data support the findings of this study are included in the main text and SI ap-pendix. All procedures of experiments are described in detail in the Materials and Methods and SI appendix.

ACKNOWLEDGEMENTS

AUTHOR CONTRIBUTIONS

JN, XQ and SvdZ conceived the experiments. SvdZ with help of XQ performed all biochemical experiments. diMe-Doxo was made by DW under supervision of HO. XQ with help of SvdZ, CZ, JB and OvT performed the mouse experiments in FVB mice. AML PDX experiments were performed by NvG and AR under supervision of LS. Analysis of AML patient data is done by XL and XQ under supervision of JL. MC38 mouse experiments were performed by SD under supervision of RA. JYS performed mouse pathology. For the echocardiography mice experiment, treatment of the mice was performed by SvdZ, SG and XQ, echography was performed by TvH under supervision of AS. JA made the endogenous scarlet-H2B cell line. Human cardiac microtissues were generated, tested and analysed by EG, MB, VO and LT under supervision of CM. The manuscript was written by XQ, SvdZ and JN with input of all authors.

DECLARATION OF INTERESTS

J. Neefjes is a shareholder in NIHM that aims to produce Acla for clinical use.

REFERENCES

1. Weiss, R. B. (1992) The anthracyclines: will we ever find a better doxorubicin?, Seminars in oncology. 19, 670-86.

2. Rayson, D., Richel, D., Chia, S., Jackisch, C., van der Vegt, S. & Suter, T. (2008) Anthracycline-trastuzumab regimens for HER2/neu-overexpressing breast cancer: current experience and future strategies, Annals of oncology : official journal of the European Society for Medical Oncology. 19, 1530-9.

3. Lotrionte, M., Biondi-Zoccai, G., Abbate, A., Lanzetta, G., D'Ascenzo, F., Malavasi, V., Peruzzi, M., Frati, G. & Palazzoni, G. (2013) Review and meta-analysis of incidence and clinical predictors of anthracycline cardiotoxicity, Am J Cardiol. 112, 1980-4.

4. Shan, K., Lincoff, A. M. & Young, J. B. (1996) Anthracycline-induced cardiotoxicity, Ann Intern Med. 125, 47-58.

5. Chatterjee, K., Zhang, J., Honbo, N. & Karliner, J. S. (2010) Doxorubicin cardiomyopathy, Cardiology. 115, 155-62.

6. Swain, S. M., Whaley, F. S. & Ewer, M. S. (2003) Congestive heart failure in patients treated with doxorubicin: a retrospective analysis of three trials, Cancer. 97, 2869-79.

7. Liu, L., Qu, Q., Jiao, W., Zhang, Y., Li, X., Ding, C. & Wu, D. (2015) Increasing aclarubicin dose in low-dose cytarabine and aclarubicin in combination with granulocyte colony-stimulating factor (CAG regimen) is efficacious as salvage chemother-

apy for relapsed/refractory mixed-phenotype acute leukemia, Leuk Res. 39, 805-11.

8. Qu, Q., Liu, L., Zhang, Y., Li, X. & Wu, D. (2015) Increasing aclarubicin dosage of the conventional CAG (low-dose cytarabine and aclarubicin in combination with granulocyte colony-stimulating factor) regimen is more efficacious as a salvage therapy than CAG for relapsed/refractory acute myeloid leukemia, Leuk Res. 39, 1353-9.

9. Sadurska, E. (2015) Current Views on Anthracycline Cardiotoxicity in Childhood Cancer Survivors, Pediatric cardiology. 36, 1112-9.

10. Mulrooney, D. A., Yeazel, M. W., Kawashima, T., Mertens, A. C., Mitby, P., Stovall, M., Donaldson, S. S., Green, D. M., Sklar, C. A., Robison, L. L. & Leisenring, W. M. (2009) Cardiac outcomes in a cohort of adult survivors of childhood and adolescent cancer: retrospective analysis of the Childhood Cancer Survivor Study cohort, Bmj. 339, b4606.

11. Grenier, M. A. & Lipshultz, S. E. (1998) Epidemiology of anthracycline cardiotoxicity in children and adults, Seminars in oncology. 25, 72-85.

12. Volkova, M. & Russell, R., 3rd (2011) Anthracycline cardiotoxicity: prevalence, pathogenesis and treatment, Current cardiology reviews. 7, 214-20.

13. Shakir, D. K. & Rasul, K. I. (2009) Chemotherapy induced cardiomyopathy: pathogenesis, monitoring and management, Journal of clinical medicine research. 1, 8-12.

14. Mistry, A. R., Felix, C. A., Whitmarsh, R. J., Mason, A., Reiter, A., Cassinat, B., Parry, A., Walz, C., Wiemels, J. L., Segal, M. R., Ades, L., Blair, I. A., Osheroff, N., Peniket, A. J., Lafage-Pochitaloff, M., Cross, N. C., Chomienne, C., Solomon, E., Fenaux, P. & Grimwade, D. (2005) DNA topoisomerase II in therapy-related acute promyelocytic leukemia, N Engl J Med. 352, 1529-38.

15. Ratain, M. J. & Rowley, J. D. (1992) Therapy-related acute myeloid leukemia secondary to inhibitors of topoisomerase II: from the bedside to the target genes, Annals of oncology : official journal of the European Society for Medical Oncology. 3, 107-11.

16. Smith, R. E., Bryant, J., DeCillis, A., Anderson, S., National Surgical Adjuvant, B. & Bowel Project, E. (2003) Acute myeloid leukemia and myelodysplastic syndrome after doxorubicin-cyclophosphamide adjuvant therapy for operable breast cancer: the National Surgical Adjuvant Breast and Bowel Project Experience, Journal of clinical oncology : official journal of the American Society of Clinical Oncology. 21, 1195-204.

17. Andre, M., Mounier, N., Leleu, X., Sonet, A., Brice, P., Henry-Amar, M., Tilly, H., Coiffier, B., Bosly, A., Morel, P., Haioun, C., Gaulard, P., Reyes, F., Gisselbrecht, C. & Groupe D'Etude Des Lymphomes De, L. A. (2004) Second cancers and late toxicities after treatment of aggressive non-Hodgkin lymphoma with the ACVBP regimen: a GELA cohort study on 2837 patients, Blood. 103, 1222-8.

18. Kayser, S., Dohner, K., Krauter, J., Kohne, C. H., Horst, H. A., Held, G., von Lilienfeld-Toal, M., Wilhelm, S., Kundgen, A., Gotze, K., Rummel, M., Nachbaur, D., Schlegelberger, B., Gohring, G., Spath, D., Morlok, C., Zucknick, M., Ganser, A., Dohner, H., Schlenk, R. F. & German-Austrian, A. (2011) The impact of therapy-related acute myeloid leukemia (AML) on outcome in 2853 adult patients with newly diagnosed AML, Blood. 117, 2137-45.

19. Hulegardh, E., Nilsson, C., Lazarevic, V., Garelius, H., Antunovic, P., Rangert Derolf, A., Mollgard, L., Uggla, B., Wennstrom, L., Wahlin, A., Hoglund, M., Juliusson, G., Stockelberg, D. & Lehmann, S. (2015) Characterization and prognostic features of secondary acute myeloid leukemia in a population-based setting: a report from

the Swedish Acute Leukemia Registry, American journal of hematology. 90, 208-14.
20. Felix, C. A. (1998) Secondary leukemias induced by topoisomerase-targeted drugs, Biochim Biophys Acta. 1400, 233-55.
21. Govindan, R. & Morgensztern, D. (2012) Devita, Hellman, and Rosenberg's Cancer: Principles and Practice of Oncology Review, Wolters Kluwer Health.
22. Tewey, K. M., Rowe, T. C., Yang, L., Halligan, B. D. & Liu, L. F. (1984) Adriamy-cin-induced DNA damage mediated by mammalian DNA topoisomerase II, Science. 226, 466-8.
23. Chen, G. L., Yang, L., Rowe, T. C., Halligan, B. D., Tewey, K. M. & Liu, L. F. (1984) Nonintercalative antitumor drugs interfere with the breakage-reunion reac-tion of mammalian DNA topoisomerase II, The Journal of biological chemistry. 259, 13560-6.
24. Pang, B., Qiao, X., Janssen, L., Velds, A., Groothuis, T., Kerkhoven, R., Nieu-wland, M., Ovaa, H., Rottenberg, S., van Tellingen, O., Janssen, J., Huijgens, P., Zwart, W. & Neefjes, J. (2013) Drug-induced histone eviction from open chromatin contributes to the chemotherapeutic effects of doxorubicin, Nature communications. 4, 1908.
25. Girling, D. J. (1996) Comparison of oral etoposide and standard intravenous mul-tidrug chemotherapy for small-cell lung cancer: a stopped multicentre randomised trial. Medical Research Council Lung Cancer Working Party, Lancet. 348, 563-6.
26. Hong, W. K., Nicaise, C., Lawson, R., Maroun, J. A., Comis, R., Speer, J., Luedke, D., Hurtubise, M., Lanzotti, V., Goodlow, J. & et al. (1989) Etoposide com-bined with cyclophosphamide plus vincristine compared with doxorubicin plus cyclo-phosphamide plus vincristine and with high-dose cyclophosphamide plus vincristine in the treatment of small-cell carcinoma of the lung: a randomized trial of the Bristol Lung Cancer Study Group, Journal of clinical oncology : official journal of the Ameri-can Society of Clinical Oncology. 7, 450-6.
27. Yang, F., Kemp, C. J. & Henikoff, S. (2013) Doxorubicin enhances nucleosome turnover around promoters, Curr Biol. 23, 782-7.
28. Nesher, E., Safina, A., Aljahdali, I., Portwood, S., Wang, E. S., Koman, I., Wang, J. & Gurova, K. V. (2018) Role of Chromatin Damage and Chromatin Trapping of FACT in Mediating the Anticancer Cytotoxicity of DNA-Binding Small-Molecule Drugs, Cancer research. 78, 1431-1443.
29. Pang, B., de Jong, J., Qiao, X., Wessels, L. F. & Neefjes, J. (2015) Chemical profiling of the genome with anti-cancer drugs defines target specificities, Nat Chem Biol. 11, 472-80.
30. Wei, G., Ni, W., Chiao, J. W., Cai, Z., Huang, H. & Liu, D. (2011) A meta-analysis of CAG (cytarabine, aclarubicin, G-CSF) regimen for the treatment of 1029 patients with acute myeloid leukemia and myelodysplastic syndrome, Journal of hematology & oncology. 4, 46.
31. Jin, J., Wang, J. X., Chen, F. F., Wu, D. P., Hu, J., Zhou, J. F., Hu, J. D., Wang, J. M., Li, J. Y., Huang, X. J., Ma, J., Ji, C. Y., Xu, X. P., Yu, K., Ren, H. Y., Zhou, Y. H., Tong, Y., Lou, Y. J., Ni, W. M., Tong, H. Y., Wang, H. F., Mi, Y. C., Du, X., Chen, B. A., Shen, Y., Chen, Z. & Chen, S. J. (2013) Homoharringtonine-based induction regi-mens for patients with de-novo acute myeloid leukaemia: a multicentre, open-label, randomised, controlled phase 3 trial, The Lancet Oncology. 14, 599-608.
32. Jonkers, J., Meuwissen, R., van der Gulden, H., Peterse, H., van der Valk, M. & Berns, A. (2001) Synergistic tumor suppressor activity of BRCA2 and p53 in a condi-tional mouse model for breast cancer, Nature genetics. 29, 418-25.
33. Ben-Yehuda, D., Krichevsky, S., Caspi, O., Rund, D., Polliack, A., Abeliovich,

3

D., Zelig, O., Yahalom, V., Paltiel, O., Or, R., Peretz, T., Ben-Neriah, S., Yehuda, O. & Rachmilewitz, E. A. (1996) Microsatellite instability and p53 mutations in therapy-related leukemia suggest mutator phenotype, Blood. 88, 4296-303.

34. Wong, T. N., Ramsingh, G., Young, A. L., Miller, C. A., Touma, W., Welch, J. S., Lamprecht, T. L., Shen, D., Hundal, J., Fulton, R. S., Heath, S., Baty, J. D., Klco, J. M., Ding, L., Mardis, E. R., Westervelt, P., DiPersio, J. F., Walter, M. J., Graubert, T. A., Ley, T. J., Druley, T., Link, D. C. & Wilson, R. K. (2015) Role of TP53 mutations in the origin and evolution of therapy-related acute myeloid leukaemia, Nature. 518, 552-555.

35. Gabizon, A., Meshorer, A. & Barenholz, Y. (1986) Comparative long-term study of the toxicities of free and liposome-associated doxorubicin in mice after intravenous administration, J Natl Cancer Inst. 77, 459-69.

36. Hanahan, D. & Weinberg, R. A. (2011) Hallmarks of cancer: the next generation, Cell. 144, 646-74.

37. Teepen, J. C., van Leeuwen, F. E., Tissing, W. J., van Dulmen-den Broeder, E., van den Heuvel-Eibrink, M. M., van der Pal, H. J., Loonen, J. J., Bresters, D., Versluys, B., Neggers, S., Jaspers, M. W. M., Hauptmann, M., van der Heiden-van der Loo, M., Visser, O., Kremer, L. C. M., Ronckers, C. M. & Group, D. L. S. (2017) Long-Term Risk of Subsequent Malignant Neoplasms After Treatment of Childhood Cancer in the DCOG LATER Study Cohort: Role of Chemotherapy, J Clin Oncol. 35, 2288-2298.

38. Henderson, T. O., Moskowitz, C. S., Chou, J. F., Bradbury, A. R., Neglia, J. P., Dang, C. T., Onel, K., Novetsky Friedman, D., Bhatia, S., Strong, L. C., Stovall, M., Kenney, L. B., Barnea, D., Lorenzi, E., Hammond, S., Leisenring, W. M., Robison, L. L., Armstrong, G. T., Diller, L. R. & Oeffinger, K. C. (2016) Breast Cancer Risk in Childhood Cancer Survivors Without a History of Chest Radiotherapy: A Report From the Childhood Cancer Survivor Study, Journal of clinical oncology : official journal of the American Society of Clinical Oncology. 34, 910-8.

39. Hequet, O., Le, Q. H., Moullet, I., Pauli, E., Salles, G., Espinouse, D., Dumontet, C., Thieblemont, C., Arnaud, P., Antal, D., Bouafia, F. & Coiffier, B. (2004) Subclinical late cardiomyopathy after doxorubicin therapy for lymphoma in adults, Journal of clinical oncology : official journal of the American Society of Clinical Oncology. 22, 1864-71.

40. Fujihira, S., Yamamoto, T., Matsumoto, M., Yoshizawa, K., Oishi, Y., Fujii, T., Noguchi, H. & Mori, H. (1993) The high incidence of atrial thrombosis in mice given doxorubicin, Toxicol Pathol. 21, 362-8.

41. Lefrak, E. A., Pitha, J., Rosenheim, S. & Gottlieb, J. A. (1973) A clinicopathologic analysis of adriamycin cardiotoxicity, Cancer. 32, 302-14.

42. Zhao, S., Wu, H., Xia, W., Chen, X., Zhu, S., Zhang, S., Shao, Y., Ma, W., Yang, D. & Zhang, J. (2014) Periostin expression is upregulated and associated with myocardial fibrosis in human failing hearts, J Cardiol. 63, 373-8.

43. Lencova-Popelova, O., Jirkovsky, E., Mazurova, Y., Lenco, J., Adamcova, M., Simunek, T., Gersl, V. & Sterba, M. (2014) Molecular remodeling of left and right ventricular myocardium in chronic anthracycline cardiotoxicity and post-treatment follow up, PloS one. 9, e96055.

44. Ogawara, D., Fukuda, M., Nakamura, Y. & Kohno, S. (2010) Efficacy and safety of amrubicin hydrochloride for treatment of relapsed small cell lung cancer, Cancer management and research. 2, 191-5.

45. Speth, P. A., van Hoesel, Q. G. & Haanen, C. (1988) Clinical pharmacokinetics of doxorubicin, Clin Pharmacokinet. 15, 15-31.

46. Wlodek, D., Banath, J. & Olive, P. L. (1991) Comparison between pulsed-field and constant-field gel electrophoresis for measurement of DNA double-strand breaks in irradiated Chinese hamster ovary cells, International journal of radiation biology. 60, 779-90.

47. Neijenhuis, S., Verwijs-Janssen, M., Kasten-Pisula, U., Rumping, G., Borgmann, K., Dikomey, E., Begg, A. C. & Vens, C. (2009) Mechanism of cell killing after ionizing radiation by a dominant negative DNA polymerase beta, DNA Repair (Amst). 8, 336-46.

48. Olive, P. L. & Banath, J. P. (2006) The comet assay: a method to measure DNA damage in individual cells, Nat Protoc. 1, 23-9.

49. Kuo, L. J. & Yang, L. X. (2008) Gamma-H2AX - a novel biomarker for DNA double-strand breaks, In vivo. 22, 305-9.

50. Suzuki, T., Minamide, S., Iwasaki, T., Yamamoto, H. & Kanda, H. (1997) Cardiotoxicity of a new anthracycline derivative (SM-5887) following intravenous administration to rabbits: comparative study with doxorubicin, Investigational new drugs. 15, 219-25.

51. Sanchez, P. V., Perry, R. L., Sarry, J. E., Perl, A. E., Murphy, K., Swider, C. R., Bagg, A., Choi, J. K., Biegel, J. A., Danet-Desnoyers, G. & Carroll, M. (2009) A robust xenotransplantation model for acute myeloid leukemia, Leukemia. 23, 2109-17.

52. Giacomelli, E., Bellin, M., Orlova, V. V. & Mummery, C. L. (2017) Co-Differentiation of Human Pluripotent Stem Cells-Derived Cardiomyocytes and Endothelial Cells from Cardiac Mesoderm Provides a Three-Dimensional Model of Cardiac Microtissue, Curr Protoc Hum Genet. 95, 21 9 1-21 9 22.

53. Giacomelli, E., Bellin, M., Sala, L., van Meer, B. J., Tertoolen, L. G., Orlova, V. V. & Mummery, C. L. (2017) Three-dimensional cardiac microtissues composed of cardiomyocytes and endothelial cells co-differentiated from human pluripotent stem cells, Development. 144, 1008-1017.

54. Guadix, J. A., Orlova, V. V., Giacomelli, E., Bellin, M., Ribeiro, M. C., Mummery, C. L., Perez-Pomares, J. M. & Passier, R. (2017) Human Pluripotent Stem Cell Differentiation into Functional Epicardial Progenitor Cells, Stem Cell Reports. 9, 1754-1764.

55. Sala, L., van Meer, B. J., Tertoolen, L. G. J., Bakkers, J., Bellin, M., Davis, R. P., Denning, C., Dieben, M. A. E., Eschenhagen, T., Giacomelli, E., Grandela, C., Hansen, A., Holman, E. R., Jongbloed, M. R. M., Kamel, S. M., Koopman, C. D., Lachaud, Q., Mannhardt, I., Mol, M. P. H., Mosqueira, D., Orlova, V. V., Passier, R., Ribeiro, M. C., Saleem, U., Smith, G. L., Burton, F. L. & Mummery, C. L. (2018) MUSCLEMOTION: A Versatile Open Software Tool to Quantify Cardiomyocyte and Cardiac Muscle Contraction In Vitro and In Vivo, Circ Res. 122, e5-e16.

56. Aapro, M., Bernard-Marty, C., Brain, E. G., Batist, G., Erdkamp, F., Krzemieniecki, K., Leonard, R., Lluch, A., Monfardini, S., Ryberg, M., Soubeyran, P. & Wedding, U. (2011) Anthracycline cardiotoxicity in the elderly cancer patient: a SIOG expert position paper, Annals of oncology : official journal of the European Society for Medical Oncology. 22, 257-67.

57. Myers, C. E., McGuire, W. P., Liss, R. H., Ifrim, I., Grotzinger, K. & Young, R. C. (1977) Adriamycin: the role of lipid peroxidation in cardiac toxicity and tumor response, Science. 197, 165-7.

58. Swain, S. M., Whaley, F. S., Gerber, M. C., Weisberg, S., York, M., Spicer, D., Jones, S. E., Wadler, S., Desai, A., Vogel, C., Speyer, J., Mittelman, A., Reddy, S., Pendergrass, K., Velez-Garcia, E., Ewer, M. S., Bianchine, J. R. & Gams, R. A. (1997) Cardioprotection with dexrazoxane for doxorubicin-containing therapy in ad-

vanced breast cancer, Journal of clinical oncology : official journal of the American Society of Clinical Oncology. 15, 1318-32.

59. Martin, E., Thougaard, A. V., Grauslund, M., Jensen, P. B., Bjorkling, F., Hasinoff, B. B., Tjornelund, J., Sehested, M. & Jensen, L. H. (2009) Evaluation of the topoisomerase II-inactive bisdioxopiperazine ICRF-161 as a protectant against doxorubicin-induced cardiomyopathy, Toxicology. 255, 72-9.

60. Myers, C., Bonow, R., Palmeri, S., Jenkins, J., Corden, B., Locker, G., Doroshow, J. & Epstein, S. (1983) A randomized controlled trial assessing the prevention of doxorubicin cardiomyopathy by N-acetylcysteine, Seminars in oncology. 10, 53-5.

61. Hashimoto, K., Ito, K. & Ishimori, Y. (1994) Novel DNA Sensor for Electrochemical Gene Detection, Analytica Chimica Acta. 286, 219-224.

62. Gabizon, A. A., Patil, Y. & La-Beck, N. M. (2016) New insights and evolving role of pegylated liposomal doxorubicin in cancer therapy, Drug resistance updates : reviews and commentaries in antimicrobial and anticancer chemotherapy. 29, 90-106.

63. van Asperen, J., van Tellingen, O., Tijssen, F., Schinkel, A. H. & Beijnen, J. H. (1999) Increased accumulation of doxorubicin and doxorubicinol in cardiac tissue of mice lacking mdr1a P-glycoprotein, British journal of cancer. 79, 108-13.

64. Steinhorst, U. H., Chen, E. P., Freedman, S. F., Machemer, R. & Hatchell, D. L. (1994) Growth inhibition of human Tenon's capsule fibroblasts and rabbit dermal fibroblasts with non-carcinogenic N-alkylated anthracyclines, Graefes Arch Clin Exp Ophthalmol. 232, 347-54.

65. Schaefer, A., Westendorf, J., Lingelbach, K., Schmidt, C. A., Mihalache, D. L., Reymann, A. & Marquardt, H. (1993) Decreased resistance to N,N-dimethylated anthracyclines in multidrug-resistant Friend erythroleukemia cells, Cancer Chemother Pharmacol. 31, 301-7.

66. Binaschi, M., Capranico, G., Dal Bo, L. & Zunino, F. (1997) Relationship between lethal effects and topoisomerase II-mediated double-stranded DNA breaks produced by anthracyclines with different sequence specificity, Molecular pharmacology. 51, 1053-9.

67. van Asperen, J., van Tellingen, O. & Beijnen, J. H. (1998) Determination of doxorubicin and metabolites in murine specimens by high-performance liquid chromatography, J Chromatogr B Biomed Sci Appl. 712, 129-43.

68. Slovak, M. L., Kopecky, K. J., Cassileth, P. A., Harrington, D. H., Theil, K. S., Mohamed, A., Paietta, E., Willman, C. L., Head, D. R., Rowe, J. M., Forman, S. J. & Appelbaum, F. R. (2000) Karyotypic analysis predicts outcome of preremission and postremission therapy in adult acute myeloid leukemia: a Southwest Oncology Group/Eastern Cooperative Oncology Group Study, Blood. 96, 4075-83.

69. Dohner, H., Estey, E. H., Amadori, S., Appelbaum, F. R., Buchner, T., Burnett, A. K., Dombret, H., Fenaux, P., Grimwade, D., Larson, R. A., Lo-Coco, F., Naoe, T., Niederwieser, D., Ossenkoppele, G. J., Sanz, M. A., Sierra, J., Tallman, M. S., Lowenberg, B., Bloomfield, C. D. & European, L. (2010) Diagnosis and management of acute myeloid leukemia in adults: recommendations from an international expert panel, on behalf of the European LeukemiaNet, Blood. 115, 453-74.

SUPPLEMENTAL INFORMATION

3

Tumor types	Saline (n=26)	Doxo (n=22)	Etop (n=28)	Acla (n=26)	Chi-square test P value
Thymic lymphoma	4 (15%)	1 (4.5%)	2 (7.1%)	2 (7.7%)	0,5571
Spindle cell sarcoma/ rhabdomyosarcoma	9 (35%)	8 (36%)	10 (36%)	13 (50%)	0,7168
Histiocytic sarcoma	3 (12%)	0 (0%)	2 (7.1%)	2 (7.7%)	0,4666
Fibrosarcoma	0 (0%)	0 (0%)	2 (7.1%)	0 (0%)	0,1409
Hemangiosarcoma	1 (3.8%)	0 (0%)	0 (0%)	1 (3.8%)	0,5880
Osteosarcoma	2 (7.7%)	1 (4.5%)	0 (0%)	3 (12%)	0,3424
Harderian gland adenoma	1 (3.8%)	0 (0%)	1 (3.6%)	2 (7.7%)	0,6161
Lung carcinoma/adenoma	6 (23%)	1 (4.5%)	4 (14%)	5 (19%)	0,3382
Adenocarcinoma/carcinosarcoma/ sarcoma of mammary gland	1 (3.8%) *(9.1%)*	11 (50%)*** *(65%)**	3 (11%)^^ *(20%)*	3 (12%)^^ *(23%)*	**<0.0001** ***0,0060***
Squamous cell carcinoma	1 (3.8%)	4 (18%)	2 (7.1%)	0 (0%)^	0,0774
Others	4 (15%)	1 (4.5%)	8 (29%)	3 (12%)	0,1090

Table S1. The spectrum and incidence of tumors observed in Trp53$^{+/-}$ FVB mice after drug treatments. *The isolated tumors were histopathologically analyzed for diagnosis. The number of animals appearing with a defined tumor type is listed in the table for each group. Of note, some mice suffered from two types of tumors at the same time. The corresponding cumulative incidence is indicated in brackets. Italic characters indicate the cumulative incidence in females, ** P = 0.008. Fisher's exact test, two-sided. Saline vs treatment, ***P = 0.0004; **P = 0.0060; Doxo vs other treatment, ^P = 0.0376, ^^P < 0.01. Not significant results are not marked by symbols.*

Figure S1. Continued (E). *Two-way ANOVA with RM, **P < 0.01; ***P < 0.001. (F) Cumulative incidence of cardiotoxicity including all observed alterations in the heart: thrombosis formation, degenerative changes of the myocytes, inflammatory infiltration and edematous changes in the myocardium or epicardium. (G) Median survival time for each group in weeks following different doses of Doxo treatment. Log-rank (Mantel-Cox) test, *P = 0.0439; **P = 0.0022. (H) Incidence rate of cardiotoxicity including all observed alterations in the Trp53$^{+/-}$ FVB mouse hearts. Cumulative incidence is indicated next to the curve. Two-way ANOVA with RM, ****P < 0.0001.*

A

- Saline (n=11)
- Doxo (n=17)
- Etop (n=15)
- Acla (n=13)

Incidence rate

11/17 = 65%****

3/15 = 20%***
3/13 = 23%**
1/11 = 9%

Time post treatment start (weeks)

B

Weeks

***
**** ns

Ctr Doxo Acla Etop

C

- Saline (n=13) ⎤ –Trp53+/+ mice
- 4xDoxo (n=6) ⎦
- 8xDoxo (n=17) ⎤ –Trp53+/- mice
- 6xDoxo (n=32) ⎦

Incidence rate

**
* ****

Time post treatment start (weeks)

D

Cumulative incidence of thrombus formation in the heart

Strain	$Trp53^{+/+}$			$Trp53^{+/-}$	
Gender	8x Saline	4x Doxo	8x Doxo	6x Saline	6x Doxo
Male	0%	33.3% **** 100%		0%	78.6%
Female	0%	0% ** 83.3%		0%	44.4%
Total	0%	16.7% **** 88.2%		0%	59.4%

E

Incidence rate

***
** **

Time post treatment start (weeks)

F

Cumulative incidence of cardiotoxicity in FVB mice

Strain	$Trp53^{+/+}$			$Trp53^{+/-}$	
Gender	8x Saline	4x Doxo	8x Doxo	6x Saline	6x Doxo
Male	0%	100%	100%	0%	85.7%
Female	0%	0%	100%	0%	72.2%
Total	0%	50.0%	100%	0%	78.1%

G

Median survival (wk)

$Trp53^{+/+}$	Saline	N.D.
	4x Doxo	21.5
	8x Doxo	17.0
$Trp53^{+/-}$	Saline	50.5
	6x Doxo	22.0

*
**

N.D. : not detectable

H

Incidence rate of cardiotoxicity

25/32 = 78.1%****

- Saline (n=26)
- Doxo (n=32)
- Etop (n=28)
- Acla (n=27)

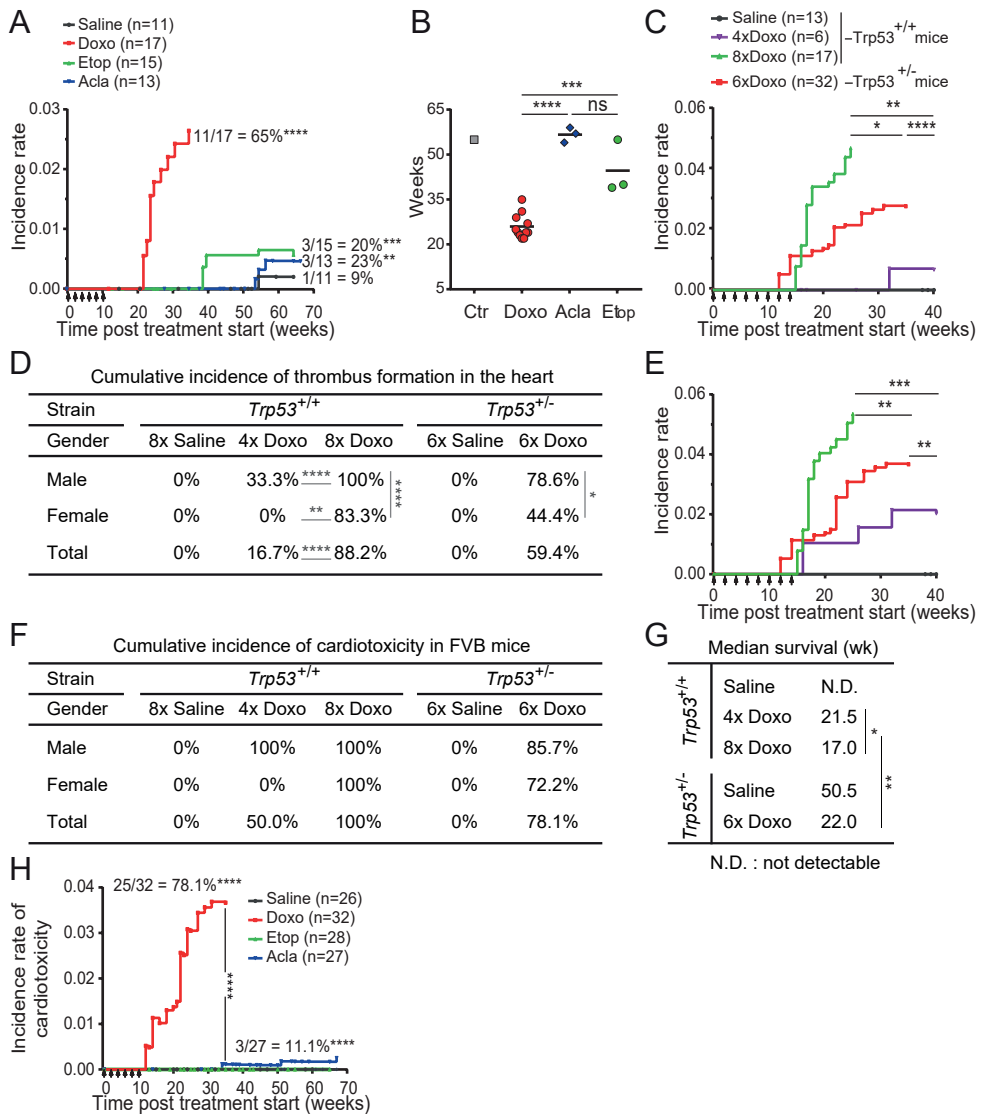****

3/27 = 11.1%****

Time post treatment start (weeks)

Figure S1. Side effects induced by Doxo treatment in FVB mice. *Trp53+/- FVB mice were i.v. injected with 5 mg/kg of Doxo, 5 mg/kg of Acla, 25 mg/kg of Etop, or 5 ml/kg of saline every two weeks for six times, whereas Trp53+/+ FVB mice were i.v. injected with 5 mg/kg of Doxo or 5 ml/kg of saline every two weeks for indicated times. Injections were indicated by arrows. (A) The incidence rate of breast cancer in Trp53+/- FVB mice. The cumulative incidence of each group is indicated next to the line. Two-way ANOVA with RM, **P < 0.01; ***P < 0.001; ****P < 0.0001. (B) The latency for breast cancer development. Unpaired t test, ***P = 0.0001; ****P < 0.0001. (C) Incidence rate of thrombus formation in the heart related to various doses of Doxo. Two-way ANOVA with RM, *P < 0.05; **P < 0.01; ****P < 0.0001. (D) Cumulative incidence of thrombus formation. Fisher's exact test, two-sided: *P < 0.05; **P < 0.01; ****P < 0.0001. (E) Incidence rate of cardiotoxicity including all observed alterations in the heart: thrombosis formation, degenerative changes of the myocytes, inflammatory infiltration and edematous changes in the myocardium or epicardium.*
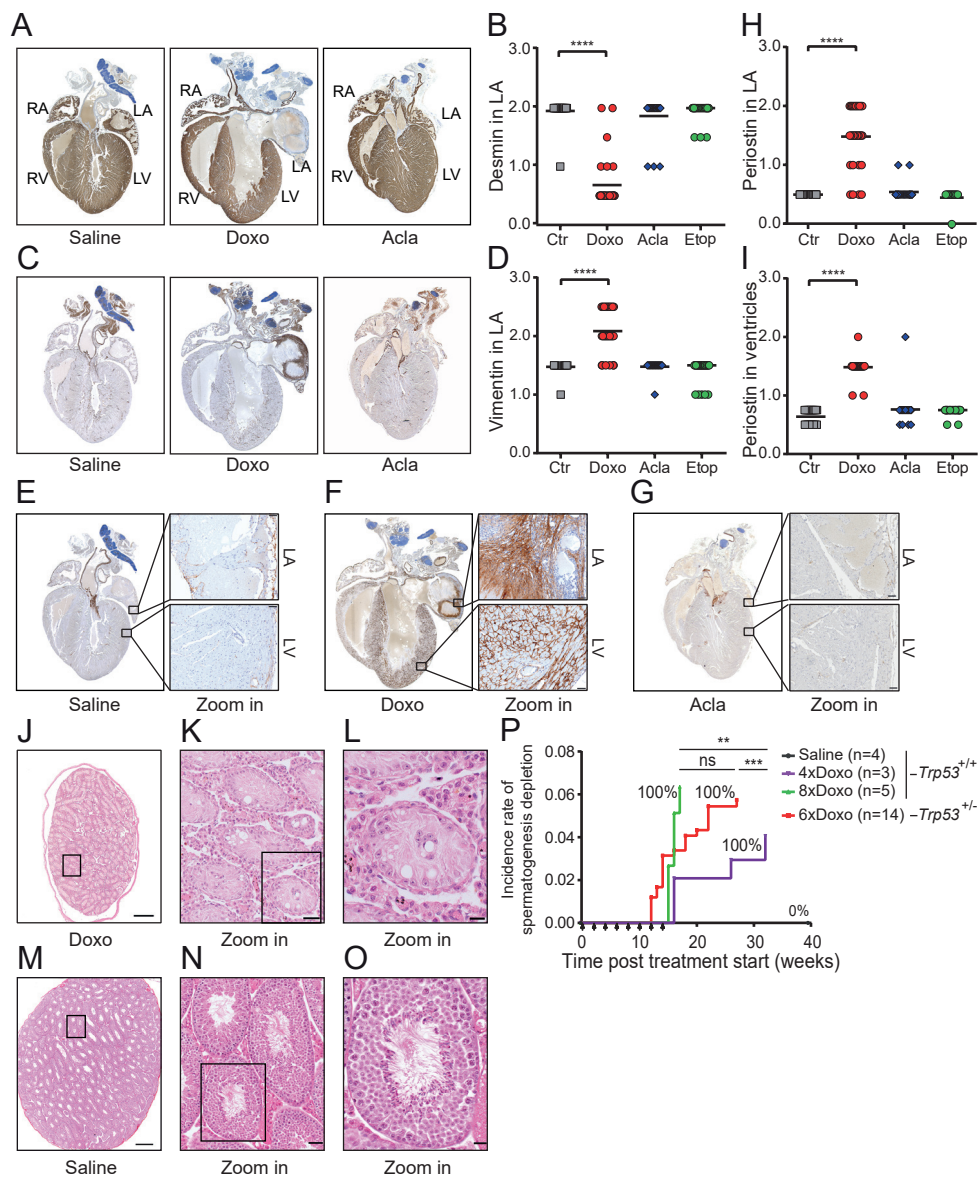
Figure S2. Cardiotoxicity and depletion of spermatogenesis by Doxo treatment in Trp53^{+/-} FVB mice. *(A) Representative Desmin staining of the hearts from saline-, Doxo- or Acla-treated mouse. RA = right atrium, RV = right ventricle, LA = left atrium, LV = left ventricle. (B) Quantification of Desmin staining in the LA. Kruskal-Wallis test, ****P < 0.0001. Ctr vs Acla or Etop is ns. (C) Representative Vimentin staining of the hearts from saline-, Doxo- or Acla-treated mouse. (D) Quantification of Vimentin staining in the LA. Kruskal-Wallis test, ****P < 0.0001. Ctr vs Acla or Etop is ns. (E) Representative Periostin staining of the heart from a saline-treated mouse. Scale bars, 50 µm. (F) Representative Periostin staining of the heart from a Doxo-treated mouse. Scale bars, 50 µm. (G) Representative Periostin staining of the heart from an Acla-treated mouse. Scale bars, 50 µm.*

Figure S2. continued. *(H) Quantification of Periostin staining in the LA. Kruskal-Wallis test, ****P < 0.0001. Ctr vs Acla or Etop is ns. (I) Quantification of Periostin staining in the ventricles. Kruskal-Wallis test, ****P < 0.0001. Ctr vs Acla or Etop is ns. (J) An overview of a section of the testis from a Doxo–treated mouse. Scale bar, 500 μm. (K) and (L) Higher magnifications from the same testis showing depletion of spermatogenesis. Scale bars, 50 μm, 20 μm, respectively. (M) An overview of a section of the testis from a saline-treated mouse. Scale bar, 500 μm. (N) and (O) Higher magnification from the same testis showing no abnormalities and normal spermatogenesis. Scale bars, 50 μm, 20 μm, respectively. (P) Depletion of spermatogenesis related to cumulative dose of Doxo. Incidence rate of spermatogenesis depletion is plotted for all groups. Cumulative incidence of spermatogenesis depletion is listed next to the line. Two-way ANOVA with RM, **P < 0.01; ***P < 0.001.*

3
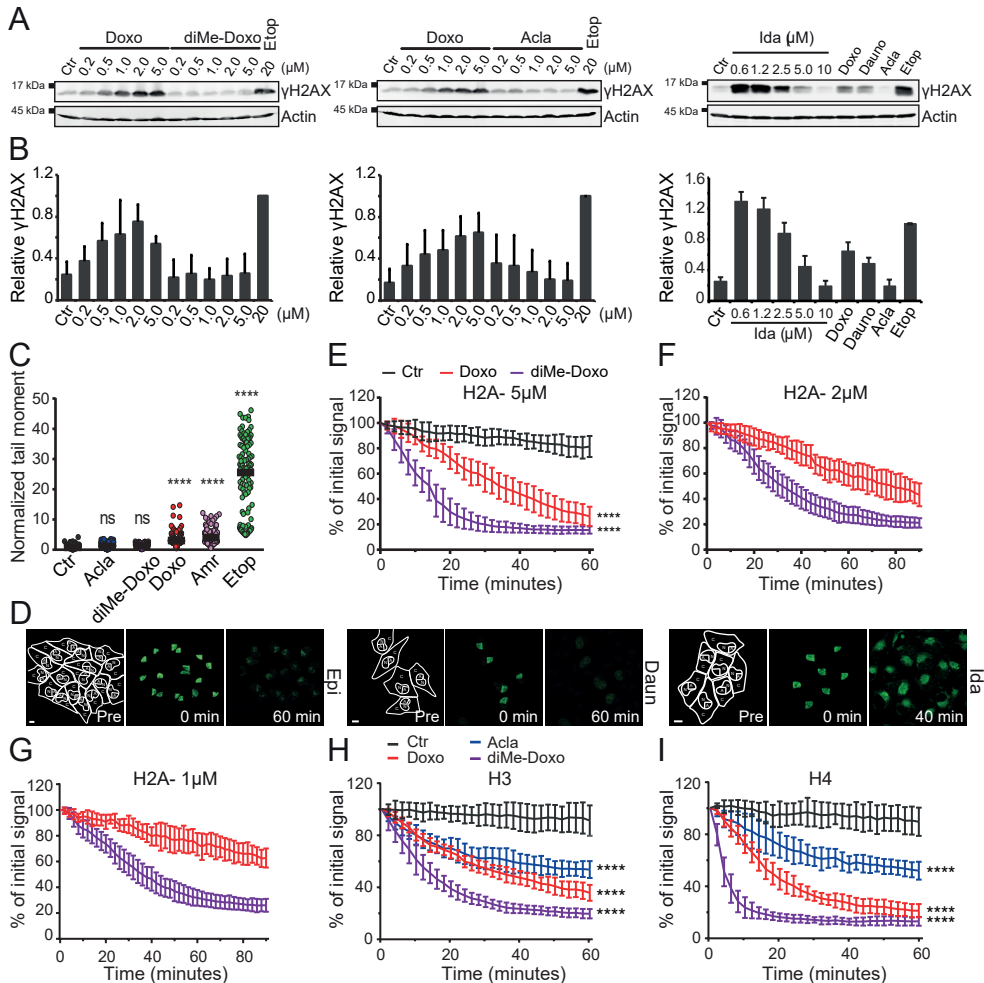
Figure S3. DNA- and chromatin-damaging activities of Topo II poisons. *(A) K562 cells were treated for 2 hours with indicated drugs and concentrations; subsequently γH2AX levels were detected by Western blot. (B) Quantification of γH2AX signal as for Figure 2C. (C) MelJuSo cells were treated for 2 hour with 10 μM of anthracyclines or 50 μM of Etop and DNA damage was examined using a neutral comet assay, normalized tail moment is plotted. Kruskal-Wallis test, ****P < 0.0001, ns, not significant.*

Figure S3. Continued. *(D) Part of the nucleus from MelJuSo PAGFP-H2A cells were photo-activated. The photo-activated PAGFP-H2A was monitored by time-lapse confocal micros-copy for 1 hour either or not in the presence of 10 µM of drugs indicated. Lines in the left panel define the cytoplasmic compartment (C), the nuclear compartment (N) and the activated area (A). Scale bar, 10 µm. (E-G) Quantification of the release of PAGFP-H2A from the photo-activated regions after the administration of different concentrations of Doxo and diMe-Doxo. Two-way ANOVA, Ctr vs Doxo or diMe-Doxo, ****P < 0.0001. (H and I) Quantification of re-lease of PAGFP-H3 (H) and H4 (I). Two-way ANOVA, ctr vs Doxo, diMe-Doxo or Acla, ****P < 0.0001.*
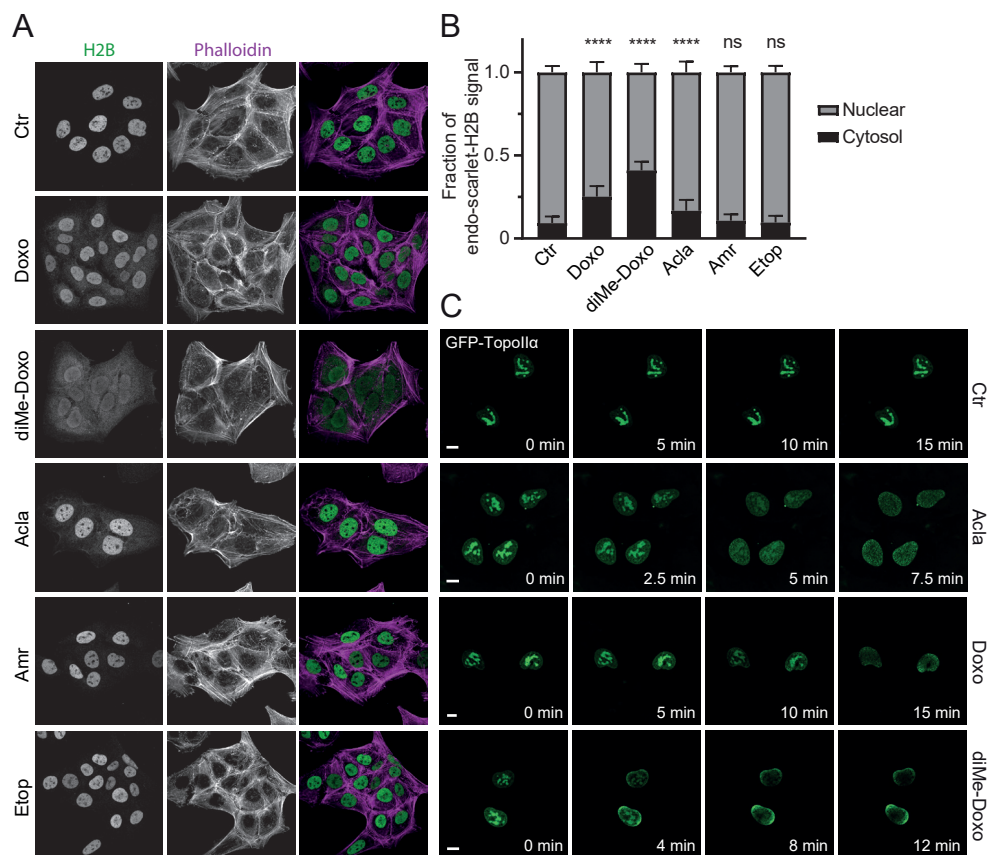
Figure S4. Chromatin damage activity by Topo II poisons causing cytosolic histone ac-cumulation. *(A) Endogenously tagged scarlet-H2B U2OS cells were treated for 1 hour with 10 µM of the indicated drugs. (B) Quantification of the nuclear versus cytosolic signal of H2B upon treatment. Two-way ANOVA, Ctr versus drug treatments, ****P < 0.0001; ns, not signifi-cant. (C) Acla, Doxo as well as diMe-Doxo relocated Topo IIα from nucleoli to chromatin. The localization of the GFP-tagged Topo IIα in MelJuSo cells was followed upon treatment with 10 µM Doxo, 10 µM diMe-Doxo or 5 µM Acla. Snapshots from movies at indicated time points. Scale bar, 10 µm.*

A

Legend: Acla, Doxo, diMe-Doxo

MCF-7 — Survival percentage vs Log[µM]

UT-SCC-8 — Survival percentage vs Log[µM]

NCI-H358 — Survival percentage vs Log[µM]

Pfeiffer — Survival percentage vs Log[µM]

Toledo — Survival percentage vs Log[µM]

MDA-MD-468 — Survival percentage vs Log[µM]

DU145 — Survival percentage vs Log[µM]

MelJuSo — Survival percentage vs Log[µM]

B

Legend: Doxo, diMe-Doxo, Acla

MelJuSo — Percentage of signal vs Minutes post addition

NCI-H358 — Percentage of signal vs Minutes post addition

MCF7 — Percentage of signal vs Minutes post addition

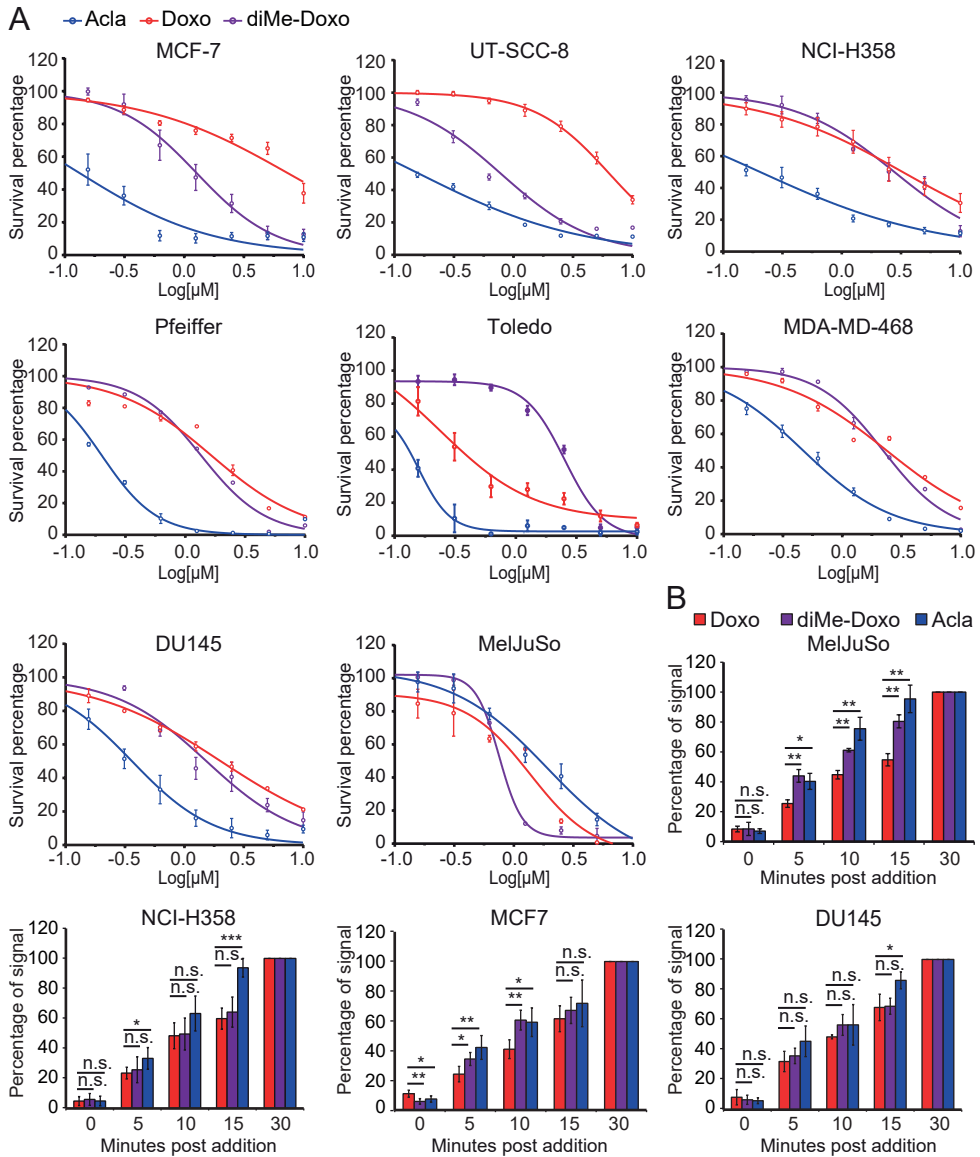DU145 — Percentage of signal vs Minutes post addition

3

Figure S5. Cytotoxicity and cellular uptake of diMe-Doxo *in vitro*. *(A) Cell viability of different cell lines. (B) The cellular uptake of drugs, measured by flow cytometry. Signal is normalized to that of the last time point. Two-tailed t-test, ns, not significant, *P < 0.05; **P < 0.01; ***P < 0.001.*

Figure S6. ROS formation and subsequent protein damage by the different Topo II poisons. *(A) ROS formation 24 hours post treatment with different concentrations of the indicated drugs was examined by flow cytometry. Two-way ANOVA, *P < 0.05; **P < 0.01; ***P < 0.001; ****P < 0.0001; ns, not significant. (B) ROS formation upon 2 hour treatment with 10 µM of anthracyclines or 50 µM of Etop. Two-way ANOVA, *P < 0.05; **P < 0.01.*
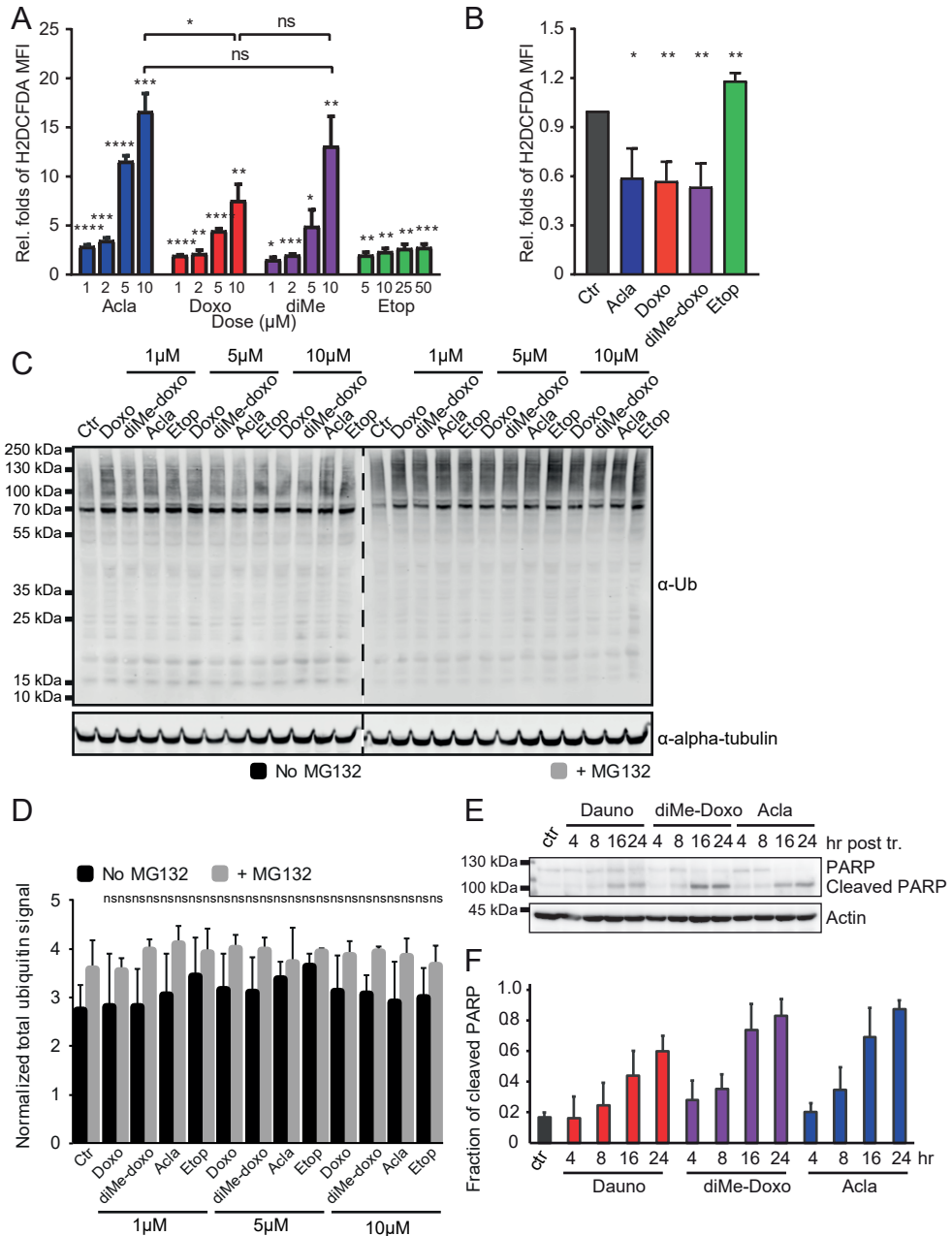
Figure S6. Continued. *(C) Total protein ubiquitination of MelJuSo cells treated for 2 hour with the indicated drugs and concentrations were examined by Western blot. Alpha-tubulin was used as a loading control. (D) Quantification of (C), total ubiquitin signal was normalized to alpha-tubulin. Ordinary one-way ANOVA, ns, not significant. (E) PARP cleavage in K562 cells analyzed by Western blot. Position of PARP and its cleaved form is indicated. Actin is used as a loading control. (F) Quantification of the fraction of cleaved PARP.*

A Survival of CR
— Acla (n=11)
— Ida (n=28)
ns *P* = 0.7576

C AML patient 3
○ Acla
○ Doxo
○ diMe-Doxo

D AML patient 4

B

Patient	Source	FAB	Age	Sex	WBC	Blasts (%)	CD34$^+$ (%)	MLL	FLT3-ITD
#1	PB	M2	66	F	114	83	14	+	+
#2	BM	N.A.	57	N.A.	N.A.	N.A.	N.A.	N.A.	N.A.
#3	PB	M3	39	M	322	67	0,01		+
#4	PB	N.A.	62	F	74	64,3	92		

Patient	NPM1	EVI1	IDH2	DNMT3A	ASXL1	Karyotype
#1			+	+		CN-X-Y
#2	N.A.	N.A.	N.A.	N.A.	N.A.	N.A.
#3	+					CN-X-Y
#4		+			+	inv(3)(q21q26.2)

N.A. = not available

E

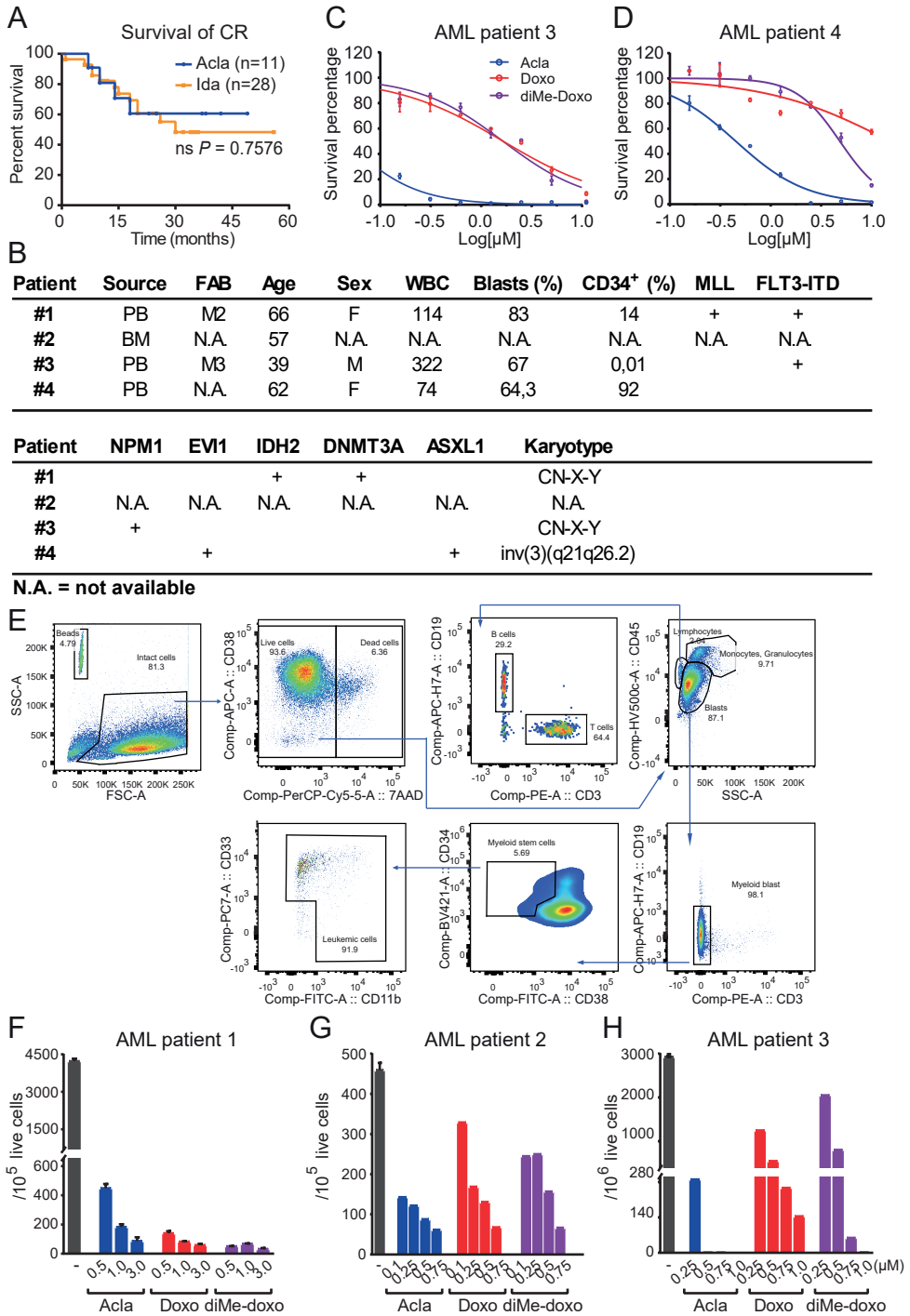**F** AML patient 1

G AML patient 2

H AML patient 3

Figure S7. *See legend on next page.*

Figure S7. diMe-Doxo and Acla are effective in human AML. *(A) Overall survival of de novo geriatric AML patients, who showed complete response after first cycle of Acla- or Ida-based treatment. Log-rank (Mantel-Cox) test. For more information on characteristics and clinical outcomes of patients, see Table S2 and S3. (B) Patient information of the four tested primary human AML samples. PB, peripheral blood; BM, bone marrow as source of the tumor materials; NA, not available. (C) and (D) Dose-dependent cell viability of human AML samples, shown as mean ± SD of technical duplicates. (E) Gating strategy of flow cytometry for immune composition analysis of the human primary AML samples. (F–H) The toxicity of drugs on leukemic cells. The data are shown as mean ± SD of technical duplicates.*

Characteristics of geriatric AML patients

Characteristics	Acla group (n = 15)		Ida group (n = 56)		*p* value
Median Age, years (range)	66	(63-71)	64	(59-70)	0.0361*
Sex					ns†
Male	6	(40%)	31	(55%)	
Female	9	(60%)	25	(45%)	
FAB subtype					ns‡
M0	0	(0%)	0	(0%)	
M1	1	(7%)	1	(2%)	
M2	0	(0%)	8	(14%)	
M4	2	(13%)	11	(20%)	
M5	2	(13%)	14	(25%)	
M6	1	(7%)	0	(0%)	
Not established	9	(60%)	22	(39%)	
Cytogenetic risk					ns‡
Favourable	2	(13%)	6	(11%)	
Intermediate	6	(40%)	19	(34%)	
Not favourable	2	(13%)	16	(28%)	
Unknown	5	(33%)	15	(27%)	
CEBPA mutation					ns‡
Mutated	2	(13%)	11	(19%)	
Wild-type	11	(73%)	44	(77%)	
Unknown	2	(13%)	2	(4%)	
FLT3-ITD mutation					ns‡
Mutated	1	(7%)	5	(9%)	
Wild-type	12	(80%)	49	(88%)	
Unknown	2	(13%)	2	(3%)	
NPM1 mutation					ns‡
Mutated	2	(13%)	19	(33%)	
Wild-type	11	(73%)	36	(63%)	
Unknown	2	(13%)	2	(4%)	
Integrated risk					0.0371‡
Favourable	3	(20%)	20	(36%)	
Intermediate	5	(33%)	4	(7%)	
Not favourable	2	(13%)	16	(28.5%)	
Unknown	5	(33%)	16	(28.5%)	

Table S2. Characteristics of *de novo* geriatric AML patients at baseline. *Data are n (%) unless otherwise stated. FAB, French–American–British. * Mann-Whitney test. † Fisher's exact test. ‡ Chi-square test. ns, not significant.*

Clinical outcomes of geriatric AML patients

Clinical outcomes	Acla group	Ida group	p value
Clinical response after one cycle			
Complete remission	11/15 (73%)	28/56 (50%)	0.1468†
Partial remission	0/15 (0%)	3/56 (5%)	>0.9999†
Non-response	4/15 (13%)	25/56 (45%)	0.2494†
Complete remission after one cycle			
Favourable cytogenetics	2/2 (100%)	3/6 (50%)	0.4643†
Intermediate cytogenetics	5/6 (83%)	10/19 (53%)	0.3449†
Unfavourable cytogenetics	2/2 (100%)	6/16 (38%)	0.1830†
Unknown cytogenetics	2/5 (40%)	9/15 (60%)	0.6169†
Overall survival			
Deaths	7/15 (47%)	25/56 (45%)	>0.9999†
Median time (95% CI; months)	18 (11.9-31.7)	14 (13.5-19.9)	0.4152‡
Cumulative dose (mg/m^2) (median, range)	63,9 (32.8-572.9)	28,5 (16.7-120.9)	<0.0001‡
TnI increase			
Events	6/8 (75%)	15/39 (38%)	0.1152†
Median time (95% CI; days)*	45 (4-194)	21 (13-25)	0.1476‡
Cumulative dose (mg/m^2) (median, range)*	84,4 (32.8-229.2)	19,2 (18-27.9)	<0.0001‡
>10% LVEF decrease			
Events	1/9 (11%)	6/33 (18%)	>0.9999†
Median time (95% CI; days)*	55	131 (48-321)	-
Cumulative dose (mg/m^2) (median, range)*	52,5	19,2 (18-27.9)	-
Adverse effects in the heart			
Events	7/11 (64%)	20/56 (36%)	0.1029†
Median time (95% CI; days)*	55 (4-194)	24 (17-56)	0.4891‡
Cumulative dose (mg/m^2) (median, range)*	58,4 (32.8-229.2)	19,3 (18.1-28.4)	0.0012‡

Table S3. Clinical outcomes of *de novo* geriatric AML patients after treatment. *Data are n/N (%) unless otherwise stated. TnI, Troponin I; LVEF, left ventricular ejection fraction; * from administration till the event happened. Adverse effects in the heart: showing either TnI increase or >10% LVEF decrease, or both. † Fisher's exact test. ‡ Mann Whitney test.*
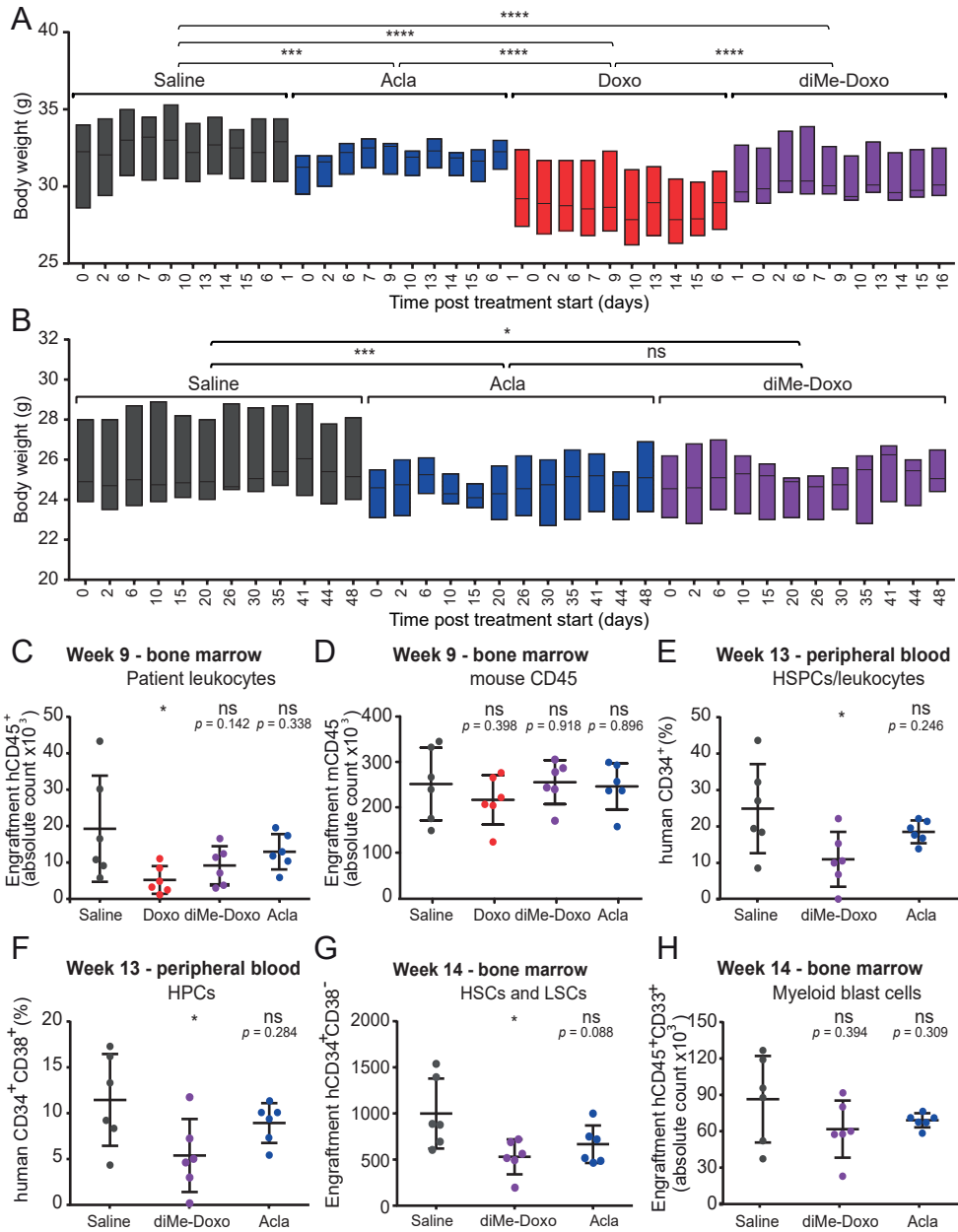
3

Figure S8. diMe-Doxo and Acla are effective in an AML PDX model. *(A) and (B) NSG mice were inoculated with primary human AML cells and treated as in Figure 3D. Body weight of the first cohort of mice (A) and the second cohort of mice (B). Shown as floating bars with maximum-median-minimum values. Two-way ANOVA with RM, *P < 0.05; ***P < 0.001; ****P < 0.0001. (C) The engraftment of human AML cells in the bone marrow of first cohort of mice at week 9, shown as absolute counts of patient leukocytes (hCD45+). Students' t-test, *P < 0.05; ns, not significant. (D) Toxicity on normal mouse leukocytes (mCD45+) in bone marrow.*

Figure S8. Continued (D). *Students' t-test, ns, not significant. (E) and (F) the percentage of human HSPCs (hCD34+ leukocytes) and HPCs (hCD34+CD38+ leukocytes) in peripheral blood of second cohort of mice at week 13. Students' t-test, *P < 0.05; ns, not significant. (G) The engraftment of human AML cells of the second cohort, the absolute counts of human HSCs and LSCs in bone marrow at week 14. Students' t-test, *P < 0.05; ns, not significant. (H) The absolute number of human myeloid blasts (hCD45+CD33+ blasts) in the bone marrow of the second cohort of mice at week 14. Students' t-test, ns, not significant.*
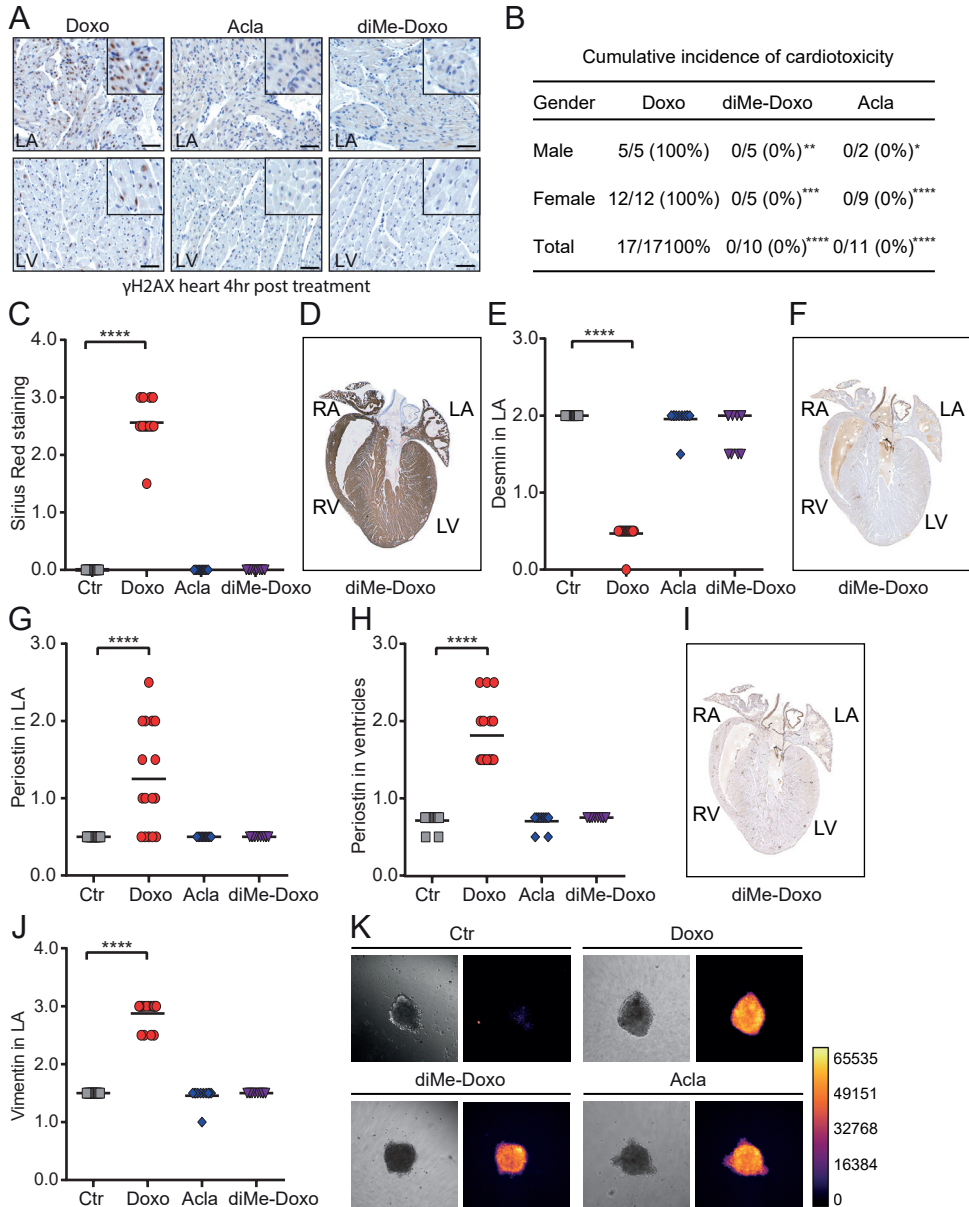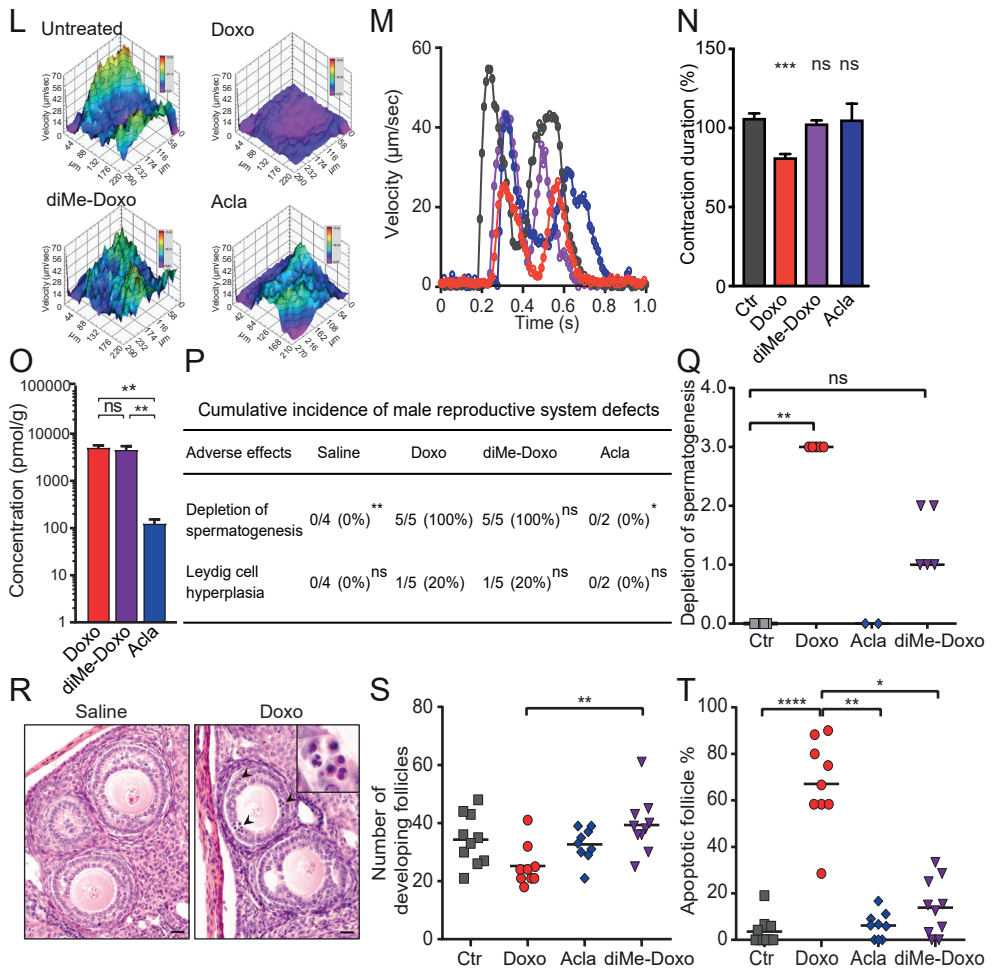
3

Figure S9. *See legend on next page.*

Figure S9. ***N,N*-dimethylation of Doxo reduces cardiotoxicity as observed for Doxo.** *(A) Wild-type FVB mice were i.v. injected with a single dose of 5 mg/kg of the indicated drugs (n = 5 per group). γH2AX staining of the heart isolated from mice 4 hours after indicated drug administration. LA = left atrium, LV = left ventricle. (B–J), Wild-type FVB mice were i.v. injected every two weeks with 5 mg/kg of Doxo or 5 mg/kg of Acla for 8 times, or with 5 mg/ kg of diMe-Doxo for 15 times. The same batch of mice as in Figure 4A–C. (B) The cumulative incidence of cardiotoxicity. Fisher's exact test, Doxo vs diMe-Doxo or Acla, *P < 0.05; **P < 0.01; ***P < 0.001; ****P < 0.0001. (C) Quantification of Sirius Red staining. Kruskal-Wallis test, ****P < 0.0001. Ctr vs Acla or diMe-Doxo is ns. (D–J), Representative IHC staining of a heart from a diMe-Doxo-treated mouse. Desmin (D), Periostin (F), Vimentin (I). (E) Quantification of Desmin staining in the LA. Kruskal-Wallis test, ****P < 0.0001. Ctr vs Acla or diMe-Doxo is ns. (G) and (H), Quantification of Periostin straining in the LA (G) and ventricles (H). Kruskal-Wallis test, ****P < 0.0001. Ctr vs Acla or diMe-Doxo is ns. (J) Quantification of vimentin staining in the LA. Kruskal-Wallis test, ****P < 0.0001. Ctr vs Acla or diMe-Doxo is ns. (K–N), hiPSC-derived cardiac microtissues were paced at 1Hz and contraction velocity was measured 24 hours post treatment. (K) Uptake of the anthracyclines is equal in hiPSC-derived cardiac microtissues. Bright field (left panels) and fluorescent image in G-LUT (right panels).*

Figure S9. Continued. *(L) Maximum velocity in µm/sec is indicated for a represented microtissue for the different treatment. (M) Quantification of (L). (N) Drug toxicity on cardiac microtissues. Contraction duration was measured 24 hours post treatment with 20 µM of the indicated drugs. Krushal-Wallis test, ***P < 0.0002. (O) Bio-distribution of drugs was determined in the heart 4 hours after administration. Same mice as A. One-way ANOVA, **P < 0.01. (P) The cumulative incidence of defects in male reproductive system. Fisher's exact test, all compared to Doxo group, *P < 0.05; **P < 0.01. (Q) Degree of the spermatogenesis depletion revealed by histopathological analysis. Kruskal-Wallis test, **P < 0.01. Ctr vs Acla is ns. (R) Representative sections of HE stained ovaries from Saline- or Doxo-treated mice. Scale bar, 20 µm. Arrows indicate apoptotic cells. (S) Quantification of the number of developing follicles in MC38-bearing mice of Exp #2. Except for primordial follicles and primary follicles, all follicles of secondary follicles, tertiary follicles (antral follicles), pre-ovulatory follicles, and large atretic follicles are regarded as developing follicles. Kruskal-Wallis test, **P < 0.01. Ctr vs Doxo, Acla or diMe-Doxo is ns. (T) Percentage of apoptotic follicles in the secondary and tertiary follicles of Exp #2. Kruskal-Wallis test, *P < 0.05; **P < 0.01; ****P < 0.0001. Ctr vs Acla or diMe-Doxo is ns.*

Movie S1: *Time-lapse confocal imaging of histone eviction upon treatment with Doxo, Amr or Etop. Cells were treated with the indicated drugs and histone eviction was followed for 1 hour after photoactivation of the indicated region by time lapse confocal microscopy. Related to Figure 2.*

Movie S2: *Time-lapse confocal imaging of histone eviction upon treatment with Doxo, diMe-Doxo or Acla. Cells were treated with the indicated drugs and histone eviction was followed for 1 hour after photoactivation of the indicated region by time lapse confocal microscopy. Related to Figure 2.*

Movie S3: *Assessment of drug toxicity by echocardiography. Wild-type FVB mice were i.v. injected with the indicated drugs for 8 times every week. Echocardiography was performed 12 weeks post start of the treatment. 3D reconstructions are shown of the heart in diastole of mice treated with the indicated drugs with the left ventricle in cyan and the left atrium in magenta. Related to Figure 4.*

Movie S4: *Drug toxicity on hiPSC-derived cardiac microtissues. hiPSC-derived cardiac microtissues were stimulated at 1Hz, and velocity of microtissue-contraction was analysed after 24 hours exposure to indicated drugs. The Horn-Schunck Vector Flow analysis method was used to detect changes in pixel displacements during contraction of the microtissues in 3D. Related to Figure 4.*

Supplemental Movies S1 - S4 can be found online: https://www.pnas.org/content/117/26/15182